The Impact of Extratropical Atmospheric Variability on ENSO: testing the Seasonal Footprinting Mechanism using Coupled Model Experiments

Michael A. Alexander
NOAA-Earth System Research Laboratory, Boulder, Colorado

Daniel J. Vimont
Department of Atmospheric and Oceanic Sciences and Center for Climatic Research, University of Wisconsin – Madison, Madison, WI

Ping Chang
Department of Oceanography, Texas A&M University, College Station, Texas

James D. Scott
NOAA/Earth System Research Laboratory, and CIRES Climate Diagnostics Center, Boulder, Colorado

Revised manuscript submitted to the Journal of Climate
January 2010

Corresponding Author Address:
Michael Alexander,
NOAA/Earth System Research Laboratory,
Physical Sciences Division,
R/PSD1,
325 Broadway,
Boulder, CO 80305-3328.
E-mail: Michael.Alexander@noaa.gov

Abstract

Previous studies suggest that extratropical atmospheric variability influences the tropics via the "seasonal footprinting mechanism" (SFM) in which fluctuations in the North Pacific Oscillation (NPO) influence the ocean via surface heat fluxes during winter and the resulting springtime subtropical SST anomalies alter the atmosphere-ocean system over the tropics in the following summer, fall and winter. Here, we test the SFM hypothesis by imposing NPO-related surface heat flux forcing in an atmospheric GCM coupled to a reduced gravity ocean model in the tropics and a slab ocean in the extratropics. The forcing is only imposed through the first winter and then the model is free to evolve through the following winter.

The evolution of the coupled model response to the forcing is consistent with the SFM hypothesis: the NPO-driven surface fluxes cause positive SST anomalies to form in the central and eastern subtropics during winter; these anomalies propagate towards the equator along with westerly wind anomalies during spring and reach the equator in summer and then amplify, leading to an ENSO event in the following winter. The anomalies reach the equator through a combination of thermodynamically coupled air-sea interactions, namely the wind evaporation SST (WES) feedback and equatorial ocean dynamics. The initial off-equatorial anomaly propagates toward the equator through a relaxation of the climatological easterlies south of the dominant SST anomalies, which leads to a reduction in upward latent heat flux. These westerly anomalies reach the equator during boreal summer where they can excite downwelling equatorial Kelvin waves. The connection between off-equatorial variations and tropical ENSO-like conditions may also occur via the excitation of westward-propagating equatorial Rossby

waves during spring, which reflect off of the western boundary as Kelvin waves, depressing the thermocline in the eastern Pacific during the following summer. NPO-related anomalies that form during the first winter in the tropical Pacific may also contribute to the development of an El Niño event in the following winter.

The imposition of the NPO-related forcing caused warming in the ENSO region in ~70% of the 60 branch simulations, and therefore the response depends on the state of the tropical atmosphere-ocean system. For years where the control simulation was poised to develop into a neutral or negative ENSO event the addition of the NPO heat fluxes tended to cause anomalous warming in the tropical Pacific in the following fall/winter; if the control was heading towards a warm ENSO event, the imposition of NPO forcing tends to reduce the amplitude of that event.

Introduction

Over the past 25 years two broad paradigms involving nonlinear/unstable or linear/stable atmosphere-ocean interactions have emerged to explain the dynamics underlying El Niño and the Southern Oscillation (ENSO). In the pioneering studies using linearly unstable models (Zebiak and Cane 1987; Battisti 1988; Schopf and Suarez, 1988), ENSO variability is self-sustained, and maintained by nonlinear interactions within the tropical Pacific. Irregular oscillations, as observed in nature, can be introduced by low-order chaos (e.g. Munnich et al. 1991; Jin et al. 1994), resulting from stronger coupling between components of the system, or by stochastic forcing (noise) that interrupts regular cycles (Blanke et al. 1997). More recent studies suggest that ENSO is linearly stable (Penland and Sardeshmukh 1995; Chang et al., 1996; Moore and Kleeman 1999; Thompson and Battisti 2000, 2001), where stochastic (external) forcing is essential for maintaining ENSO variability. Several sources of stochastic forcing have been proposed including westerly wind bursts in the central/western equatorial Pacific (e.g. Wyrki 1975; Vecchi and Harrsion 2000; McPhaden 2004; Seiki and Takayabu 2007) the Madden and Julian Oscillation (e.g. Lau and Chan 1986, 1988; Moore and Kleeman 1999; Zavala-Garay et al. 2008) and variability originating in midlatitudes that subsequently influences westerly wind bursts (Yu And Reinecker 1998; Nakamura et al. 2006, 2007)

Variability initiated in the North Pacific has the potential to influence the tropical Pacific on interannual to decadal time scales via both the ocean and the atmosphere. In the ocean, the extratropics can impact the tropics via the subtropical cell, a shallow meridional overturning circulation. Fluctuations in the temperature and salinity created by air-sea interaction in midlatitudes can be advected to the tropics within the thermocline (the lower

layer of the subtropical cell) and then upwell to the surface when they reach the equator (e.g. Gu and Philander 1997). Changes in extratropical winds can also alter the overall strength of the subtropical cell, altering the volume of cold water reaching the equator (Kleeman et al. 1999; McPhaden and Zhang 2002). Alternatively, upper ocean anomalies can be carried from higher latitudes to the tropics by westward propagating Rossby waves which transfer their energy to equatorward propagating Kelvin waves at the western boundary (Lysne et al. 1997). In the atmosphere, the response to slowly varying SST anomalies in the Kuroshio Extension region can extend into the tropics, thereby affecting the trade winds and decadal variability (Barnett et al. 1999; Pierce et al. 2000).

Midlatitude-to-tropics atmospheric connections may evolve over several seasons and involve additional portions of the climate system. Based on diagnostics of an extended CSIRO coupled general circulation model (CGCM) simulation, Vimont et al. (2001, 2003a) identified the “seasonal footprinting mechanism” (SFM) where air-sea interaction in the subtropics during the warm season links extratropical atmospheric variability in one winter with tropical variability in the following winter (Fig. 1). Specifically, fluctuations in the North Pacific Oscillation (NPO, Walker and Bliss 1932; Rogers 1981; Linkin and Nigam 2008), the second leading internal atmospheric mode over the North Pacific in winter, imparts an SST "footprint" onto the ocean via changes in the surface heat fluxes. The NPO consists of a meridional dipole in sea level pressure (SLP) over the central Pacific with centers at approximately 35°N and 60°N; when low pressure occupies the southern lobe of the NPO, the anomalous winds are from the west opposing the trade winds over the central and eastern subtropical Pacific, reducing the wind speed and upward latent flux, thereby warming the underlying ocean. The reverse set of processes

occurs during the opposite phase of the NPO. The SST footprint, which maximizes in late winter/early spring, persists through summer in the subtropics. The atmosphere responds to these SSTs and further interacts with the tropical ocean. The resulting atmospheric circulation includes zonal wind stress anomalies that extend onto the equator in the central and west Pacific. The stress anomalies excite a response in the equatorial ocean that influences the sea surface temperature (SST) and thermocline depth in the central and eastern equatorial Pacific in the subsequent winter. Vimont et al. (2001, 2003a) concluded that the SFM was an important source of external forcing for interannual ENSO variability and decadal to inter-decadal tropical variability in the CSIRO CGCM. SLP and SST precursors that resembled those associated with the NPO in the winter prior to ENSO's peak were also found in the NCAR CCSM2 (Anderson and Maloney 2006).

The SFM appears to occur in nature as well. Vimont et al. (2003b) and Anderson (2003, 2004) found statistically significant links between the NPO (and the Western Pacific Pattern, its signature in the upper troposphere; Hsu and Wallace 1985) in winter, SSTs in the subtropical North Pacific and winds in the western tropical Pacific during spring and summer, and SSTs in the ENSO region in the subsequent winter. Several studies have used linear inverse models (LIMs) derived from simultaneous and lagged covariance statistics of observed SST anomalies to better understand and predict ENSO (e.g. Penland and Magorian 1993; Penland and Sardeshmukh 1995); the springtime SFM SST pattern closely resembles the "optimal structure", the pattern identified in LIMs as the most likely to grow into a large ENSO event (Penland and Sardeshmukh 1995; Xue et al. 1997; Thompson and Battisti 2001; Alexander et al. 2008). In addition, there is a close correspondence between the development of SST anomalies predicted by LIM and the

evolution of the atmosphere-ocean system indicated by the SFM prior to ENSO events (Alexander et al. 2008).

The SFM also influences the latitude of the tropical meridional SST gradient and the intertropical convergence zone (ITCZ): the ITCZ is displaced towards (away from) the hemisphere with anomalously warm (cold) water in the subtropics and the associated winds flow across the anomalous SST gradient from the negative towards and over the positive SSTA. The variations in the meridional SST gradient and the ITCZ, termed the "merdional mode" (MM) by Chiang and Vimont (2004), has been well documented in the Atlantic over the past 30 years (e.g. Hastenrath and Heller, 1977; Xie and Carton, 2004) but was only recently uncovered in the Pacific after accounting for the dominant ENSO signal. In the Pacific the MM exhibits SST anomalies of one sign extending southwestward from Baja California to the central-western equatorial Pacific with anomalies of the opposite sign in the eastern equatorial Pacific. Chang et al. (2007) and Zhang et al. (2009a, b) present both observational and modeling evidence that the MM is a thermodynamic coupled mode independent of ENSO, and that the MM plays an important role in initiating ENSO events.

While the seasonal footprinting mechanism has been diagnosed in models and observations, several questions remain regarding the scope of the processes involved and its overall relationship to ENSO. For example, since ENSO influences the atmosphere-ocean system over the North Pacific for an extended period of time (e.g. Trenberth et al. 1998; Alexander et al. 2002), is the SFM truly an independent means of forcing ENSO or is it at least partly a component of the ENSO cycle? By what means do the ocean anomalies persist and propagate during the warm season? Do they feed back on the

atmospheric circulation in the tropical Pacific? If the SFM does initiate ENSO events, does its efficacy depend on the state of the tropical Pacific? And finally, what is the overall relationship between the SFM, MM and ENSO?

To examine these questions Vimont et al. (2009; Vimont, Alexander and Fontaine, VAF from here on) conducted atmospheric GCM – slab ocean model simulations to investigate the tropical Pacific response to mid-latitude atmospheric variability. Heat flux anomalies associated with the NPO during boreal winter were used to force the ocean in an ensemble of model simulations, after which the forcing was terminated and the coupled model was free to evolve. The SST and wind anomalies continued to amplify in the tropical Pacific after the imposed forcing was shut off, due to feedbacks between the surface wind, evaporation, and SST (WES feedback), and by changes in the shortwave radiative heat flux. In the Northern Hemisphere, the response to warm subtropical SSTs includes southwesterlies over and to the southwest of the SST maxima, which slows the trade winds and reduces the upward latent heat flux, warming the ocean and hence leading to positive WES feedback. This thermodynamic coupling results in southwestward development of SST anomalies and an associated equatorward shift in the surface zonal wind anomalies, consistent with previous studies of WES feedback (Xie and Philander 1994; Liu and Xie 1994; Xie 1996) and with studies that examined the tropical air-sea interaction in response to extratropical variability (Xie 1999; Wu and Li 2007).

In this study, we impose the same NPO surface heat flux forcing as used by VAF but in a coupled model where the ocean contains the dynamics necessary to simulate ENSO. The model, described in section 2, consists of an AGCM that is anomaly coupled to a reduced gravity ocean (RGO) model in the tropics and a slab elsewhere over the ocean.

The experiment design includes a long control integration and 60 branch simulations from the control, which include additonal NPO-related heat flux forcing (section 2). The results, obtained from the difference between the control and branch integrations, are presented in section 3 and summarized and discussed in section 4.

2. Model and Experiment design

a. Coupled model

The coupled model, described in detail by Zhang et al. (2009a), consists of the NCAR Community Climate Model version 3 (CCM3) coupled to an extended 1.5 layer reduced gravity ocean (RGO) model in the tropics and a slab mixed-layer (ML) model in the extratropics. CCM3, described by Kiehl et al. (1998), is a spectral AGCM that employs T42 truncation (2.8° lat x 2.8° lon) with 18 vertical levels. The model includes parameterizations for radiation, convection, boundary layer, and the diagnostic treatment of clouds; the land surface characteristics and sea ice extent are specified to follow the observed mean seasonal cycle.

The RGO model has been used extensively to study ENSO (e.g. Zebiak and Cane, 1987; Battisti 1988). The formulation and parameters used here are from Chang (1994). The model consists of an upper layer, which includes a fixed depth surface mixed layer, overlaying a deep motionless layer. The thermocline is located at base of the upper layer (depth h) and the surface currents consist of a surface Ekman component and a geostrophic component related to the gradient h. The surface layer temperature (equivalent to the SST) depends on advection by surface currents, upwelling and heat fluxes with the atmosphere but does not influence the ocean dynamics. The upwelling is based on the divergence of the surface currents. The model resolution is 1º latitude by 2º longitude and

its domain extends from 30ºN-30ºS in all ocean basins. The extratropical ML depth, which varies spatially but not temporally, is obtained from the annual average mixed layer depth estimated by Monterey and Levitus (1997). There is no smoothing of the SST anomalies across the RGO-ML boundary.

The RGO and ML are anomaly coupled to the CCM3: wind stress anomalies about the AGCM climatology are passed to the RGO model, the surface heat flux anomalies are passed to both the RGO and ML models, while the RGO-ML models transfer the SST anomalies back to the atmosphere. Observed climatological values are added to the anomalies to make the full fields prior to exchanging them between models. The montly SST and surface flux climatologies are obtained from Reynolds and Smith (1994) and the ECMWF reanalysis (Uppala et al. 2005), respectively**.** A seasonally varying flux correction is also applied to the ocean to keep the SST close to its observed state.

The CCM3-RGO model simulates many aspects of both the MM and ENSO reasonably well, including their temporal and spatial structures, as well as their phase-locking to the seasonal cycle (Chang et al. 2007 and Zhang et al. 2009a). However, it underestimates the amplitude of ENSO variability by about 20% and its period by ~6 months.

Here, we examine a 100-year control (Cntrl) CCM-RGO-ML simulation to determine the extent to which the SFM occurs in the model. First, the wintertime NPO is defined in the model as the second empirical orthogonal function (EOF) of North Pacific (20°N-90°N, 110°E-70°W) SLP during NDJFM. The simulated NPO, shown by the concurrent regression of SLP values on the NPO time series [the second principle component (PC) of SLP in NDJFM], strongly resembles its counterpart in nature with a meridional dipole

structure over the central North Pacific. (c.f. Rogers 1981;Vimont 2003b; Linkin and Nigam, 2008). Concurrent regressions of the net surface heat flux (Q_{net}), and lagged regression of SST and surface winds, also shown in Fig. 1, follow the SFM paradigm: strong fluxes in the subtropical eastern Pacific associated with the southern lobe of the NPO (Fig. 1a); the formation of SST and wind anomalies that develop in winter and into spring in the subtropics (Fig. 1b&c); wind anomalies that extend southwestward toward the equator in summer (Fig. 1d); and to the development of an ENSO event in the subsequent fall/winter (Fig. 1e). The SST values in Fig. 1b resemble the MM with anomalies of opposite sign on the equator and from 10°N-20°N in the eastern half of the basin. The *h* values also shown in Fig. 1, are suggestive of a La Niña–like state during the first winter, with negative (shallower) anomalies in the east and positive anomalies in the west, that evolve towards a El Nino-like state by the following winter with a deeper thermocline in the central equatorial Pacific.

b. Model experiments

Although the statistical analysis identifies the SFM in the CCM-RGL-ML simulation, there remains ambiguity surrounding its underlying cause (e.g. the NPO signal may be a response to some feature of the ENSO-cycle). Thus, we test the SFM hypothesis by conducting experiments in which an external forcing is added to the ocean components of the CCM-RGO-ML model. The imposed forcing represents the net surface heat flux (Q_{net}) anomalies associated with the NPO during boreal winter. In nature and/or coupled models, the NPO-related fluxes contain forcing associated with internal atmospheric variability, feedback from the ocean, and NPO-related variability driven by anomalies in other parts

of the climate system, which could include ENSO. To cleanly separate the part of the NPO forcing that is due to *intrinsic atmospheric variations*, the NPO-related heat fluxes were extracted from a 200-yr NCAR Community Atmospheric Model version 3 (CAM3) simulation with repeating climatological SSTs as boundary conditions. A different analysis technique applied to observations yields a very similar structure and amplitude of NPO-related heat flux variations (see VAF for a comparison between the two methods).

The NPO-related heat fluxes are identified through application of EOF analysis to the winter (NDJFM) averaged SLP anomalies from the uncoupled CAM3 simulation over the North Pacific domain. As in the CCM3-RGO-ML model, the NPO is identified by the second EOF, which explains 19% of the variance, and is well separated from the first EOF (the Aleutian Low) and higher order EOFs. The NPO-related SLP/Q_{net} fields from CAM3, obtained by regressing the SLP and Q_{net} anomalies onto the second PC, are similar to those in nature as well as in the CCM3-RGO-ML model (c.f. Fig. 1 in VAF with our Fig. 1a). Since the NPO is similar in the two models and VAF isolated the intrinsic NPO variability, we use the Q_{net} forcing obtained from CAM3 in this study. The imposed heat flux forcing used here (Fig. 2) is derived by doubling the Q_{net} values regressed onto the second SLP PC (twice those shown in Fig. 1b of VAF). In these idealized experiments, we have utilized strong forcing (a two standard deviation anomaly from the mean) to emphasize the footprinting mechanism relative to the background noise. The forcing is in accordance with the "negative" phase of the NPO, with low pressure south of 45ºN (as in Fig. 1a), consistent with Linkin and Nigam (2008) and the nomenclature used to describe the North Atlantic Oscillation (NAO)

The experiment consists of 60 branch simulations from the Cntrl, each initialized with conditions on 1 November from the first 60 years of the 100-year integration. As a result of linearly interpolating monthly input values to the model time step, the amplitude of the heat flux forcing increases from half strength on 1 Nov to full strength by mid-Nov, and decreases from full strength in mid-Mar to zero by mid-Apr. The model simulations continue with unperturbed fluxes through the following Apr (18 months total). The imposed forcing is identical in each of the branch runs and is added to the Pacific from 20ºS-60ºN. An additional set of 10 simulations was conducted where the heat flux forcing was applied from 10ºN-60ºN (100% north of 9.7ºN, 50% at 9.7ºN, 0% south of 9.7ºN). The results are presented as the differences between the Exp simulations from the corresponding periods in the Cntrl.

The experiment design will still include some redundancy between the imposed forcing and internally generated NPO variability. Ensemble averaging across the relatively large number of simulations will emphasize the forced model response; VAF found that the experimental design was appropriate for addressing the NPO's influence on tropical climate variability. Differences in the evolution of individual ensemble members, however, may indicate what aspects of the background variability, including the amplitude of the NPO and the state of the tropical Pacific ocean, are important for the development of ENSO events.

3. Results

a. NPO-forced climate anomalies

The evolution of the model in response to the imposed NPO forcing is depicted in Fig. 3, which shows the ensemble averaged Exp – Cntrl (Δ) for SST, surface winds, and latent heat flux (Q_{lh}, which is positive into the ocean and does not include the imposed forcing) during JFM(0), AMJ(0), JAS(0) and OND(1). Regions where the ensemble average of the 60 Exp simulations are significantly different from the control at the 95% level as indicated by the Student's t-test are stippled. The SST difference (or anomalies) during JFM(0) reflects the direct response to the oceanic heat flux forcing (compare Fig. 2 with Fig. 3 top left panel), which includes warm water that extends both northeastward and westward from Hawaii (~20ºN, 150ºW) and cold water to the south of Baja California and in the western North Pacific. The atmospheric flow is generally towards the warm water and the heat fluxes tend to damp the SST anomalies as the anomalously warm (cold) water loses more (less) heat to the atmosphere. A dynamic ocean response begins to develop by JFM(0), with negative thermocline depth (h) anomalies between approximately 7°N-20°N in the western Pacific and modest positive h anomalies in the the central and eastern equatorial Pacific with a maximum at ~4°N (Fig. 4a). Most of these thermocline depth changes appear to be driven by the local Ekman pumping with a deeper thermocline ($\Delta h > 0$) associated with downward Ekman pumping ($\Delta w_{ek} < 0$) and vice versa (Fig. 4). Given these changes in the atmosphere and ocean, it is apparent that ΔSST also includes anomalies generated by air-sea interaction in addition to those directly due to the imposed forcing.

The response continues to evolve once the forcing has ended by mid April: during AMJ(0) the initial NPO-driven SST signal over the northeast Pacific decreases but warm water extends further into the tropics in the central Pacific, with small positive anomalies

extending onto and south of the equator in the vicinity of 165ºW [consistent with the downward Q_{lh} anomalies during JFM(0) and AMJ(0)]. A cyclonic atmospheric circulation is centered at approximately 18ºN, 170ºW with strong southwesterlies in the tropical west Pacific (0º-15ºN, 140ºE-170ºW) and northeasterlies extending across much of the Pacific from 20ºN-30ºN. In response to the winds, the thermocline deepens from 2ºN-7ºN across the western half of the Pacific, while the positive anomalies on the equator at ~165ºW and the negative anomalies further north have also increased in amplitude (Fig. 4b).

The southwesterly flow in the subtropics opposes the mean trades, reducing the wind speed (U) and thus the evaporation; indeed ΔQ_{lh} exceeds 10 Wm^{-2} near 10ºN between 160ºE and 170ºW despite positive ΔSST in the region. Decomposing the wind speed and specific humidity (q) difference across the sea surface into their mean, obtained from the control, and departure from the control (Δ) indicated that the wind speed fluctuations are primarily responsible for ΔQ_{lh} within ~25º of the equator (not shown). The ΔQ_{lh} variability associated with the q fluctuations were of weaker amplitude and generally damped the ΔSST, except in the eastern equatorial Pacific. These interactions between SST, winds and Q_{lh} are consistent with WES feedback, which is maximized in the tropical western Pacific during boreal spring due to the seasonal cycle in background winds and the strength of the atmospheric response to SSTs (VAF). WES feedback was also identified as key driver of SST variability in the central and western tropical Pacific of the CCM3 by Mahajan et al. (2009a), although humidity fluctuations were also found to be important, for example by causing SST anomalies to extend from the extratropics to the subtropics (Mahajan et al. 2009b).

The difference in precipitation (P) between the Exp and Cntrl attains maximum amplitude during AMJ(0), when the precipitation increases (decreases) in the central tropical (western equatorial) Pacific (Fig. 5). These dipole precipitation anomalies are similar to those associated with the MM but located further north and west (c.f. Chiang and Vimont 2004). Positive ΔP coincides with the convergence of the surface wind (Fig. 3). The shortwave fluxes at the surface (not shown) are collocated but of opposite sign to ΔP (i.e. less precipitation, lower cloud amount, more sunlight reaching the surface and vice versa) and thus warm the ocean during AMJ(0) between about 5ºS and 10ºN in the west Pacific. While the structure of the latent heat and shortwave fluxes differ, both act to warm the ocean in the vicinity of 5ºN, 170ºE. The cooperating influence of shortwave and latent heat fluxes is consistent with results from Chiang and Vimont (2004), as well as VAF.

The SST anomalies initially driven by the imposed NPO forcing continue to decrease in the subtropics and northeast Pacific through JAS. However, air-sea interaction amplifies the anomalous westerly wind, SST and h on the equator, which are maximized in the western, central and eastern portions of the basin respectively. The wind anomalies, can excite equatorial Kelvin waves that propagate eastward depressing the thermocline in the central and eastern Pacific, which in turn increase SSTs in these areas presumably by the eastward advection of warm water and the reduction of upwelling. These anomalies continue to grow during OND, resulting in an ENSO-like structure throughout the tropics. Once an ENSO-like structure forms, the equatorial anomalies will continue to develop through a positive "Bjerknes" feedback between warm equatorial SST, relaxed trade winds, and a deepening thermocline (Neelin et al. 1998). This description is

consistent with the composite analysis of the MM-induced ENSO evolution in Zhang et al. (2009a).

Overall, Figs. 3-5 indicate that the evolution of the CCM-RGO-ML system both during and after the NPO forcing is applied is consistent with the SFM hypothesis: *(i)* the NPO forces SST anomalies to form in the eastern subtropics during winter; *(ii)* these SST anomalies propagate towards the equator along with westerly wind anomalies during spring; *(iii)* the SST and wind anomalies reach the equator in summer and *(iv)* air-sea interaction amplifies the anomalous westerly wind on the equator where they will continue to develop through a positive Bjerknes feedback between warm equatorial SSTs, relaxed trade winds and a deepening thermocline, leading to a fully developed ENSO event in the following winter. Nearly all of these features are statistically significant at the 95% level.

One factor that complicates the interpretation of our findings is that the NPO forcing extends to 20ºS and although the imposed flux anomalies are small south of ~10ºN ($|Q_{net}|<$ ~5 Wm^{-2}, see Fig. 2), they may directly impact equatorial dynamics, thus bypassing air-sea interaction in the subtropics. We addressed this issue by performing an additional set of 10 simulations where the NPO forcing was applied north of 10ºN. The results (not shown) were similar those in Figs. 3-5, where positive SST and wind anomalies formed and then amplified in the tropical Pacific during spring and summer and El Niño conditions followed in fall and winter – indicating that subtropical air-sea interactions are essential for the SFM, induced by the NPO, to influence ENSO.

Another complicating factor is that the flux forcing is only associated with the negative phase of the NPO. Thus, we performed another set of 10 simulations using the fluxes shown in Fig. 2 but with the opposite sign. The evolution of the model response to this

"positive" phase of the NPO is similar to that presented in Figs. 3-5 but with the sign reversed (not shown). By the winter of year 1, the model response is La Niña like with SST anomalies < -0.6°C over much of the equatorial Pacific (Fig. 6). While, there are some differences in the amplitude and pattern of the ΔSST to the two phases of the NPO (forcing compare Fig. 6 and Fig. 3 bottom left), this may be primarily due to internal fluctuations in the climate model rather to nonlinearities in the response to the NPO; isolating the nonlinear signal would likely require an extremely large ensemble of simulations with forcings of different amplitudes associated with both phases of the NPO.

We examine the evolution of the NPO-induced response further using Hövmoller diagrams constructed with pentad averaged model output. To highlight the evolution of the SFM, the Hövmoller path has a "j" shape that has been rotated by 90° (Fig. 7), i.e. it begins at 25°N, 155°W (point 0), extends southwestward to 12°N, 165°W (5), then due south to 0° (10) and finally due east along the equator to 85°W (26). The ensemble averaged Exp-Cntrl values shown for SST, Q_{lh} and U in Fig. 7 are three-point averages including the points along and perpendicular to the transect line. In response to the imposed forcing, the ΔSST (contours in Fig. 7a,b) increases from Nov(0) through Feb(0) and remain above 0.6°C through April north of ~18°N (points 0-4). During Feb(0)-Jun(0) positive (negative) wind speed (Q_{lh}) anomalies are located over the positive ΔSST, points 0-4. The stronger winds and warmer SSTs both contribute to enhanced upward latent heat flux ($\Delta Q_{lh} < 0$), through more turbulent mixing in the atmosphere (stronger winds) and an increased vertical humidity gradient (warmer SSTs), damping the underlying ΔSST. Positive ΔQ_{lh} and negative ΔU values between points 5-9, concurrent with the fluxes damping the NPO-forced anomalies albeit at a reduced amplitude, result in ΔSST values that decrease in

magnitude as they propagate towards the equator (down and to the right in Fig. 7a,b) with ΔSST > 0.2° arriving at position 10 during Jun-Jul(0). The negative wind speed anomalies, indicative of westerly wind anomalies, along with positive heat flux anomalies propagate onto the equator and are located there through summer. The ΔSST subsequently amplifies and spreads eastward along the equator reaching a maximum of ~0.5°C in the central-east Pacific (points 10-22) from Nov(1)-Jan(1), while the positive ΔU and negative ΔQ_{lh} remain in the central Pacific (points 10-15) through the winter of year 1.

A second propagating signal is seen in all three fields in Fig. 7: the anomalies start in the eastern equatorial Pacific in spring (points 22-25) and move rapidly westward reaching the central Pacific (points 10-12) by summer. The SST, U and Q_{lh} anomalies are in quadrature, with $-\Delta U$ and $+\Delta Q_{lh}$ ($+\Delta U$ and $-\Delta Q_{lh}$) located to the west (east) of the +ΔSST, consistent with thermodynamic air-sea interaction contributing to westward propagation of the anomalies. The ΔQ_{lh} anomalies are too weak to explain the ΔSST, but strong zonal current anomalies associated with this feature (not shown), indicates that equatorial dynamics likely plays an important role in its evolution. These westward propagating SST, Q_{lh} and U anomalies merge with those that moved equatorward from the subtropical North Pacific (position 5-10) from Jun(0)-Sep(0).

The evolution of Δh in Fig. 4 indicates a westward expansion of the positive thermocline depth anomalies from approximately 2°N-7°N from JFM(0) to AMJ(0) and eastward movement of depth anomalies along the equator from JFM(0) through OND(1). In addition, ENSO is known to involve westward propagating Rossby waves, which are centered around 5° latitude for the first baroclinic mode, and southward and eastward propagating Kelvin waves, located along the western boundary and equator, respectively.

Thus, we construct a 3-panel Hövmoller diagram of five day running mean Δh with transects centered at 5°N, along the western boundary at 132.5°E, and on the equator (Fig. 8). The transect along 5°N is reversed (east on the left) to aid in tracking anomalies that travel counter clockwise around the basin. Westward propagation of thermocline anomalies is readily apparent along 5°N in the perturbed simulations. In particular, positive Δ*h* values which form in the central Pacific (~160°W) during Mar-Apr(0) reach the western boundary by summer, consistent with the group velocity of the first baroclinic Rossby wave (about 1 m s^{-1}). Upon reaching the boundary the anomalies rapidly propagate south and then eastward along the equator, consistent with Kelvin wave dynamics. The equatorial Kelvin wave(s) appear to propagate all the way to the eastern boundary over ~2 months during spring and summer but the magnitude of the anomalies are not of uniform across the equator. They may constructively interfere with the thermocline anomalies generated by local westerly wind anomalies in the vicinity of 180°-160°W, where the latter initially developed during Mar(0). In addition, Δ*h* decreases in amplitude on the equator from approximately 140°W in Jun(0) to the dateline in Aug(0) followed by an increase in amplitude slightly to the east. The latter results from a shoaling of the thermocline in advance (to the west) and a deepening behind the westward propagating ΔSST (Fig. 7). Thus, additional processes may contribute to the SFM in the CCM-RGO model, including oceanic Rossby waves that reflect off the western boundary and SST-wind anomalies that propagate rapidly westward along the equator.

b. ENSO Characteristics

The impact of the imposed forcing on the development of ENSO, is further explored in Fig. 9, which shows the difference in SST during NDJ(1) between each of the 60 Exp branch simulations and the corresponding period for the Cntrl in the Nino 3.4 region. The mean difference between the two is 0.47°C (significant at the 99% level). The SSTs warmed in the Nino 3.4 region in the subsequent winter after the forcing was applied in 43 of the 60 cases (~72%), while the 17 cases that cooled are dispersed throughout the ensemble. Including the forcing added 11 more warm events, as indicated by the number of ensemble members in which the Nino 3.4 ΔSST > 0.89, 1σ of SST averaged over NDJ in the Cntrl.

Are there additional factors that influence the extent to which the NPO-related forcing impacts the development of ENSO? We address this question via a scatter plot of ΔSST during NDJ(1) verses the SST departures relative to the long-term mean in the Cntrl (denoted by a $'$) for the corresponding period (Fig. 10). Thus, the x-axis in Fig. 10 indicates whether or not the control simulation develops into an ENSO event, and the y-axis indicates the departure from the control trajectory, due to imposition of the NPO-related heat flux. The NPO-driven response in the 60 cases, numbered in Fig. 10 by their corresponding years in the control simulation, vary greatly from year to year of the integration, e.g. the largest ΔSST values (red dots in Fig. 10) are not clustered in consecutive years. Thus, the response does not appear to be strongly influenced by decadal variability in the Cntrl integration. The ENSO response is also relatively independent of the strength of the NPO forcing in the Cntrl, as the correlation between the NPO time series in NDJFM(0) and the Nino3.4 ΔSST in NDJ(1) is only 0.13 with no nonlinear relationship apparent from the scatter plot (not shown).

If the response to the imposed forcing was linear (independent of the conditions in the control) plus noise, then the points would appear as scatter about a horizontal line with the average ΔSST value in Fig. 10. However, a more complex response maybe anticipated, i.e. the efficacy of the stochastic forcing likely depends on the state of the tropical Pacific. One possible cause of a nonlinear response is saturation, i.e. the total Nino 3.4 temperature has a maximum value and thus ΔSST could be large and positive when a La Niña event is expected in the Cntrl simulation (negative SST'), positive and moderate amplitude for events that would have been neutral ENSO events, and asymptote toward zero when an El Niño event was expected from the Cntrl simulation (positive SST'). The points in Fig. 10 do display a negative slope (correlation of -0.44), indicating that the NPO forces the system towards an El Niño (ΔSST > 0) when it had negative SST′ in the Cntrl simulation. However, there is not clear evidence for saturation for large SST′ but rather an indication that the imposed forcing disrupted strong El Niño events in the Cntrl, since ΔSST<0 when SST′>0. The true dependence of the response on the climate state, however, may require a very large ensemble to be well defined. In addition, the application of a constant forcing in the Exp simulations may result in a different mean state that could impact the overall variability and hence the mean spread in ΔSST.

An intriguing aspect of the NPO-induced responses shown in Fig. 10 are the branch simulations that developed very large ΔSSTs during NDJ(1) when the Cntrl was slightly cold or near neutral (red points). We explore the causes for these eight "warm" cases by compositing their associated SST′ and ΔSST fields and comparing them to composites of eight cases with similar SST′ values but near zero ΔSST in NDJ(1), termed "neutral" cases (shown by blue points in Fig. 10). The composite SST′ and h' fields for NDJ in Yr(0) and

Yr(1) for the neutral and warm cases are shown in Fig. 11 along with the ΔSST and Δ*h* in NDJ(1), where the arrows between panels illustrates the progression of the system with and without forcing. Consistent with Fig. 10, weak La Niña conditions occur in the tropical Pacific during NDJ(1) in the Cntrl for both the neutral (Fig. 11b) and warm (Fig. 11e) cases. In the neutral composite, El Niño conditions were present in the Cntrl during NDJ(0) (Fig. 11a) and the imposition of the NPO forcing has little impact on the system, as indicated by the negligible ΔSST and Δ*h* in the eastern equatorial Pacific during NDJ(1) (Fig. 11c). Given that El Niño events decay in less than one year and there are two or more years between events, the addition of NPO forcing appears to be ineffective in generating El Niño conditions in the subsequent winter when a warm event is currently in progress. In the absence of stochastic forcing, this version of the model maintains weak ENSO variability, i.e. the ENSO mode is in a weakly nonlinear state (Chang et al. 2007; Zhang et al. 2009b), so during large El Niño events the imposition of external forcing does not appear strong enough to veer the system from its trajectory towards a La Niña. In contrast, the evolution of Cntrl simulation from the years used in the warm composite, shows modest negative SST′s in the central Pacific and a deeper thermocline in the western Pacific in the winter of yr(0) as well as yr(1). The addition of the NPO forcing results in a very strong ΔSST and Δ*h* response that resembles a mature El Niño event over the entire domain by NDJ(1) (Fig. 11f). This suggests that the SFM may be an especially effective trigger for warm events when the tropical Pacific would otherwise tend towards consecutive La Niñas. The combined influence of the SFM with a deeper thermocline in the west Pacific on ENSO is also consistent with Anderson (2007) who found that anomalous low pressure in the northern subtropics is a more effective at initiating an El

Niño event when combined with an increase in heat content in the western equatorial Pacific a year before an event.

In addition to the initial state in the Cntrl, the evolution of anomalies in the tropical Pacific may also depend on both local and remote air-sea interactions induced by the imposed forcing, even though the latter is identical in all of the cases. As a result, the Exp-Cntrl values may differ between cases at the end of the forcing period, which could then amplify with time as the system freely evolves over the next 12 months. We investigate this idea by showing ΔSST and Δh during Mar(0), near the end of the period with anomalous forcing, for the neutral and warm composites in Fig. 12. While positive ΔSSTs are found in the vicinity of Hawaii in both sets of composites, differences between the two occur in multiple locations. The positive ΔSST during Mar(0) in subtropical North Pacific extend further west between 10°N-20°N in the neutral compared with the warm composite. The negative ΔSST near Central America are of larger amplitude and greater extent in the neutral cases, while the large negative values that occur along the entire southern coast of Asia in the warm composite are absent from the neutral composite.

The Δh during Mar(0) are also markedly different in the two composites (Fig. 12c,d). In the neutral case, the forcing results in a deeper thermocline on the equator in the central Pacific and a shallower thermocline off the equator in the western Pacific. In the warm composite, the thermocline is deeper off the equator, with maxima along 5°N and 5°S from 160°E-150°W and shallower across most of the basin between 10°-20°N. The Δh > 0 at ~5° latitude, are indicative of downwelling gravest mode Rossby waves, which in the "delayed oscillator mechanism" (Schopf and Suarez 1988; Battisti and Hirst 1989) propagate westward to the western boundary, move equatorward along the boundary and

then east along the equator depressing the thermocline and creating ENSO conditions approximately 6-10 months later (consistent with Fig. 8). The anomaly structure in Fig. 12d, is also consistent with the recharge/discharge ENSO paradigm (Jin 1997; Meinen and McPhadden 2000), where changes in heat storage, indicated by thermocline depth anomalies, are nearly zonally uniform at all latitudes with positive values located off the equator prior to ENSO events. At the peak of the event, h is deep in the east and shallow in the west along the equator, which is also the structure of Δh in NDJ(1) (not shown but similar in pattern to the anomalies in Fig. 4d but with 2-3 times the amplitude).

While its unclear which aspects of the model's base state at the start of the integration or the evolution of the response during the forcing period are critical to the formation of an El Niño event by the following winter, the ΔSST in the warm composite during Mar(0) strongly resemble the Meridional Mode, which has been identified as a precursor for ENSO events (Chiang and Vimont 2004; Chang et al. 2007, Zhang et al. 2009a,b). Both display SST anomalies of one sign that extend southwestward from Baja California to the equator between 150°E-180° and anomalies of the opposite sign occur near the equator in the eastern half of the basin. Thus, NPO-related forcing may be more effective in exciting El Niño events if tropical air-sea interaction results in a strong projection on the MM during boreal spring.

4. Discussion and Conclusions

The seasonal footprinting mechanism was examined using an atmospheric GCM coupled to a Cane and Zebiak type reduced gravity ocean model in the tropics and a slab ocean model in the extratropics. The impact of extratropical variability on the

development of ENSO events is investigated through a comparison of a control simulation with 60 branch simulations that include identical external forcing. The forcing consists of the surface heat flux anomalies associated with the North Pacific Oscillation, the second leading SLP mode over the extratropical Pacific. The forcing, derived from the negative phase of the NPO (high pressure over Alaska and low pressure near Hawaii), warms the central subtropical Pacific through winter but is terminated by mid April.

The results show that boreal wintertime midlatitude atmospheric variability associated with the NPO is capable of exciting an ENSO-like response in the tropical Pacific beginning in boreal spring/summer, and amplifying through the following fall and winter. Off-equatorial anomalies reach the equator through a combination of thermodynamically coupled air-sea interactions, namely the WES feedback and equatorial ocean dynamics. The initial off-equatorial anomaly propagates toward the equator through a relaxation of the climatological easterlies south of the dominant SST anomalies, which leads to a reduction in upward latent heat flux. These westerly anomalies reach the equator during boreal summer (Fig. 7), where they can excite downwelling equatorial Kelvin waves. The connection between off-equatorial variations and tropical ENSO-like conditions may also occur via the excitation of westward-propagating equatorial Rossby waves during the boreal spring immediately following the wintertime imposed forcing. These Rossby waves reflect off of the western boundary as equatorward propagating Kelvin waves, depressing the thermocline in the eastern Pacific during the following summer (Fig. 8). The Rossby wave mechanism appears to be especially prominent in the cases with the largest response (Fig. 12) and resembles the precursor to El Nino events in the delayed oscillator and recharge/discharge paradigms for ENSO. The depressed thermocline is associated with

warmer SST and likely initiates a Bjerknes-type feedback that allows El Niño conditions to continue to develop.

In addition to the off-equatorial anomalies that take several months to reach the equator, there are also SST/wind/thermocline depth anomalies that form on the equator in the east Pacific (~90°W) in spring and propagate rapidly westward reaching the central Pacific (~160°W) by summer (Fig. 7). While the role of this feature in the SFM is unclear, it resembles the "mobile mode" described by Mantua and Battisti (1995) and the "Pacific Ocean basin (POB) mode" identified by Jin et al. (2003) and Kang et al. (2004) and has been found in observations, the Cane and Zebiak model and GCMs. In addition, these studies have found that the equatorial SST anomalies are primarily driven by anomalous zonal currents, which is consistent with the large zonal currents associated with the westward propagating anomalies excited by the NPO forcing in our experiments. Analyses of shallow water models (Mantua and Battisti 1995; Kang et al. 2004) indicate that the time scale of the POB mode, which is independent of the ~4 yr ENSO mode, is approximately 9-12 months and is set by the time it takes the gravest free Rossby wave and coastal/equatorial Kelvin waves to propagate around the basin. Air-sea coupling destabilizes the POB mode, allowing it to grow rapidly for certain base states, and influence SST anomalies in the ENSO region.

While the imposition of the NPO-related forcing caused warming in the ENSO region in ~70% of the 60 branch simulations, the impact of the forcing on individual events depends on the state of the tropical ocean / atmosphere system. For years where the control simulation was poised to develop into a neutral or negative ENSO event the addition of the NPO heat fluxes tended to cause anomalous warming relative to the control

simulation in the tropical Pacific in the following fall/winter. On the other hand, if the control trajectory were heading towards a warm ENSO event, the imposition of NPO-related heat fluxes tends to reduce the amplitude of that event. This is consistent with results in Zhang et al. (2009b; see their Fig. 9), who found that ~70% of ENSO events were initiated by the MM in a long control integration. A possible explanation is that the MM-induced warming in the north tropical Pacific can work in concert with an existing cold anomaly in the equatorial Pacific to enhance the meridional SST gradient, causing a stronger thermodynamic feedback that acts to intensify or at least persist the MM. In contrast, a preexisting warming condition near the equator works against the MM development because it tends to weaken the meridional SST gradient.

The spatial structure of NPO-related heat flux anomalies in the tropical Pacific bears a strong resemblance to the Meridional Mode. While this suggests that the MM is simply due to the SFM, other studies have found that the MM exists independent of external forcing (Xie 1997, 1999; Okajima et al. 2003; Chang et al. 2007; Kossin and Vimont, 2007; Zhang et al. 2009 a,b). The MM dynamics include an equatorward and westward propagation of SST anomalies (Liu and Xie 1994; VAF; Zhang et al. 2009a), which is consistent with the evolution of SST anomalies in the present analysis. As such, the SFM may be a means of exciting the tropical Pacific MM, the dynamics of which ultimately lead to tropical Pacific variations that amplify via the Bjerknes feedback. In this way, the SFM, MM and ENSO fit together in a dynamic framework where the SFM plays a dominant role in forcing the MM, whereas the MM acts as a conduit through which the extratropical atmosphere influences ENSO.

Changes in other NPO-related variables could also impact the tropical Pacific. For example, changes in zonal wind stress associated with the NPO could directly impact equatorial ocean dynamics, instead of as part of the response to the subtropical SSTs generated by the surface heat fluxes. In addition, the SFM is clearly not the only means of exciting tropical Pacific variability. As shown in Fig. 10, there is considerable ENSO variability that is not explained by the imposed NPO-related heat fluxes. In particular, the importance of westerly wind bursts (WWB) in the initiation of ENSO events, has been highlighted by various authors (e.g. McPhadden 1988; Vecchi and Harrsion 2000; McPhaden 2004; Seiki and Takayabu 2007). The spatial structure of SST anomalies that are associated with periods of excessive westerly wind burst activity bears a strong resemblance to the NPO-related SST anomalies (Vecchi and Harrison 2000). An examination of high pass filtered daily output from the CCM-RGO model, however, did not show an increase in the number and/or intensity of WWBs in the NPO-forced simulations relative to the control. Nevertheless, the relationship between WWB's and the SFM should be more fully explored in coupled GCMs and observations.

Acknowledgements

We thank Bruce Anderson for his insightful comments on a previous version of the manuscript. This research was supported by grants from the NOAA Climate Program Office's Climate Variability and Predictability program and the NSF Climate and Large-Scale Dynamics program.

References

Alexander, M. A., L. Matrosova, C. Penland, J. D. Scott, and P. Chang, 2008: Forecasting Pacific SSTs: Linear Inverse Model Predictions of the PDO. *J. Climate*, **21,** 385-402.

Alexander, M. A., I. Blade, M. Newman, J. R. Lanzante, N.-C. Lau, and J. D. Scott, 2002: The atmospheric bridge: the influence of ENSO teleconnections on air-sea interaction over the global oceans. *J. Climate*, **15,** 2205-2231.

Anderson, B. T., 2003: Tropical Pacific sea surface temperatures and preceding sea level pressure anomalies in the subtropical north Pacific. *J. Geophys. Res.*, **108**, 4732, doi:10.1029/ 2003JD003805.

Anderson, B. T., 2004: Investigation of a large-scale mode of ocean–atmosphere variability and its relation to tropical Pacific sea surface temperature anomalies. *J. Climate*, **17,** 4089–4098.

Anderson, B. T., 2007: On the joint role of subtropical atmospheric variability and equatorial subsurface heat content anomalies in initiating the onset of ENSO events. *J. Climate*, **20,** 1593-1599.

Anderson, B. T., and E. Maloney, 2006: Interannual tropical Pacific sea-surface temperatures and preceding sub-tropical sea level pressures in the NCAR CCSM2.0. *J. Climate*, **19,** 998-1012.

Barnett, T., D. W. Pierce, M. Latif, D. Dommonget, and R. Saravanan, 1999: Interdecadal interactions between the tropics and the midlatitudes in the Pacific basin. *Geophys. Res. Lett.*, **26,** 615-618.

Battisti, D. S., 1988: Dynamics and thermodynamics of a warming event in a coupled tropical atmosphere-ocean model. *J. Atmos. Sci.*, **45,** 2889-2919.

Battisti, D. S., and A. C. Hirst, 1989: Interannual variability in the tropical atmosphere-ocean system: influence of the basic state and ocean geometry. *J. Atmos. Sci.*, **45,** 1687-1712.

Blanke, B., J. D. Neelin, and D. Gutzler, 1997: Estimating the effect of stochastic wind stress forcing on ENSO irregularity. *J. Climate*, **10,** 1473–1486.

Chang, P., 1994: Seasonal cycle of sea surface temperature and the mixed layer heat budget in the tropical Pacific Ocean. *Geophys. Res. Lett.*, **20,** 2079-2082.

Chang, P., L. Ji, H. Li, and M. Flügel, 1996: Chaotic Dynamics versus stochastic processes in El Niño-Southern Oscillation in coupled ocean-atmosphere models. *Physica D*, **98,** 301-320.

Chang, P., L. Zhang, R. Saravanan, D. J. Vimont, J. C. H. Chiang, and H. S. L. Ji, and M.

K. Tippett, 2007: Pacific meridional mode and El Niño–Southern Oscillation. *Geophys. Res. Lett.*, **34,** L16608, doi:10.1029/2007GL030302.

Chiang, J. C., and D. J. Vimont, 2004: Analogous Pacific and Atlantic meridional modes of tropical atmosphere–ocean variability. *J. Climate*, **17,** 4143–4158.

Gu, D. and S. G. H. Philander, 1997: Interdecadal climate fluctuations that depend on exchanges between the tropics and extratropics. *Science*, **275,** 805-807.

Hastenrath, S., and L. Heller, 1977: Dynamics of climatic hazards in northeast Brazil. *Quart. J. Roy. Meteor. Soc.*, **103,** 77-92.

Hsu, H.-H. and J. M. Wallace, 1985: Vertical structure of wintertime teleconnection patterns. *J. Atmos. Sci.*, **42,** 1693–1710.

Jin, F.-F., 1997: An equatorial ocean recharge paradigm for ENSO. Part I: Conceptual model. *J. Atmos. Sci.*, **54,** 811–829.

Jin, F.-F., J.-S. Kug, S.-I. An, and I.-S. Kang,, 2003: A near-annual coupled ocean–atmosphere mode in the equatorial Pacific Ocean. *Geophys. Res. Lett.*, **30,** 1080, doi:10.1029/2002GL015983.

Jin, F.-F., D. Neelin, and M. Ghil, 1994: El Niño on the devil's staircase: annual

subharmonic steps to chaos. *Science*, **264,** 70-72.

Kang, I.-S., J.-S. Kug, S.-I. An, and F.-F. Jin, 2004: A near-annual Pacific Ocean basin mode. *J. Climate*, **17,** 2478–2488.

Kiehl, J. T., J. J. Hack, G. B. Bonan, B. A. Boville, and P. J. Rasch, 1998: The National Center for Atmospheric Research Community Climate Model: CCM3. *J. Climate*, **11,** 1131-1149.

Kleeman, R., J. P. McCreary, and B. A. Klinger, 1999: A mechanism for the decadal variation of ENSO. *Geophys. Res. Lett.*, **26,** 1743 – 1747.

Kossin, J. P. a. D. J. V., 2007: A more general framework for understanding Atlantic hurricane variability and trends. *Bull. Amer. Meteor. Soc.*, **88,** 1767–1781.

Lau, K.-M., and P. H. Chan, 1986: The 40–50 day oscillation and the El Niño/Southern Oscillation: A new perspective. *Bull. Amer. Meteor. Soc.*, **67,** 533–534.

Lau, K.-M., 1988: Intraseasonal and interannual variations of tropical convection: A possible link between 40–50 day oscillation and ENSO? *J. Atmos. Sci.*, **45,** 506–521.

Linkin, M. E., and S. Nigam, 2008: The North Pacific Oscillation–West Pacific Teleconnection Pattern: mature-phase structure and winter impacts. *J. Climate*, **21,**

1979-1997.

Liu, Z., and S.-P. Xie, 1994: Equatorward propagation of coupled air-sea disturbances with application to the annual cycle of the eastern tropical Pacific. *J. Atmos. Sci.*, **51,** 3807-3822.

Lysne, J. A., P. Chang, and B. Giese, 1997: Impact of the Extratropical Pacific on Decadal Variability in the Tropics, *Geophys. Res. Lett.*, **24**, 2589-2592.

Mahajan S., R. Saravanan, P. Chang, 2009a: The role of the wind-evaporation-sea surface temperature (WES) feedback in air–sea coupled tropical variability, *Atmos. Res*., 94, 19-36, doi:10.1016/j.atmosres.2008.09.017.

Mahajan S., R. Saravanan, P. Chang, 2009b: The wind-evaporation-sea surface temperature (WES) feedback as a thermodynamic pathway for the equator-ward propagation of high latitude sea-ice induced cold anomalies. *J. Climate*. Submitted.

Mantua, N. J., and D. S. Battisti, 1995: Aperiodic variability in the Zebiak-Cane coupled ocean-atmosphere model: ocean-atmosphere interactions in the western equatorial Pacific. *J. Climate*, **8,** 2897-2927.

McPhadden, M. J., 2004: Evolution of the 2002/03 El Niño. *Bull. Amer. Met. Soc.*, **8,** 677-695.

Mcphaden, M. J., H. P. Freitag, S. P. Hayes, B. A. Taft, Z. Chien, and K. Wyrtki, 1988: The response of the equatorial Pacific Ocean to a westerly wind burst in may 1986. *J. Geophys. Res.*, **93,** 10589–10603.

McPhaden, M. J., and D. Zhang, 2002: Slowdown of the meridional overturning circulation in the upper Pacific Ocean, *Nature*, **415,** 603 – 608.

Meinen, C. S., and M. J. McPhadden, 2000: Observations of warm water volume changes in the equatorial Pacific and their relationship to El Niño and La Niña. *J Climate*, **13,** 3551–3559.

Monterey, G. I. and S. Levitus, 1997: *Climatological Cycle of Mixed Layer Depth in the World Ocean*. Vol. Atlas 14, U.S. Gov. Printing Office, NOAA NESDIS, 5, 87 pp.

Moore, A. M. and R. Kleeman, 1999: Stochastic forcing of ENSO by the intraseasonal oscillation. *J. Climate*, **12,** 1199–1220.

Munnich, M., M. A. Cane, and S. E. Zebiak,, 1991: A study of self-excited oscillations of the tropical ocean–atmosphere system. *J. Atmos. Sci.*, **48,** 1238–1248.

Nakamura, T., Y. Tachibana, M. Honda, and S. Yamane, 2006: Influence of the Northern Hemisphere annular mode on ENSO by modulating westerly wind bursts. *Geophys.*

Res. Lett., **33,** L07709, doi:10.1029/2005GL025432.

Nakamura, T., Y. Tachibana, and H. Shimoda, 2007: Importance of cold and dry surges in substantiating the NAM and ENSO relationship. *Geophys. Res. Lett.***,** L22703, doi:10.1029/2007GL031220.

Neelin, J. D., D. S. Battisti, A. C. Hirst, F. F. Jin, Y. Wakata, T. Yamagata and S. Zebiak, 1998: ENSO theory. *J. Geophys. Res.*, **103,** 14,261-14,290.

Okajima, H., S.-P. Xie, and A. Numaguti, 2003: Interhemispheric coherence of tropical climate variability: Effect of climatological ITCZ. *J. Meteor. Soc. Japan*, **81,** 1371-1386

Penland, C. and T. Magorian, 1993: Prediction of Niño 3 sea surface temperatures using linear inverse modeling. *J. Climate*, **6,** 1067-1076.

Penland, C. and P. D. Sardeshmukh, 1995: The optimal growth of tropical sea surface temperature anomalies. *J. Climate*, **8,** 1999-2024.

Pierce, D. W., T. P. Barnett, and M. Latif, 2000: Connections between the Pacific Ocean tropics and midlatitudes on decadal timescales. *J. Climate*, **13,** 1173-1194.

Reynolds, R. W. and T. M. Smith, 1994: Improved global sea surface temperature analyses using optimum interpolation. J. Climate, 7, 929-948.

Rogers, J. C., 1981: The North Pacific Oscillation. *J. Climatol.*, **1,** 39-52.

Schopf, P. S., and M. J. Suarez, 1988: Vacillations in a coupled ocean-atmosphere model. *J. Atmos. Sci.*, **45,** 549-566.

Seiki, A., and Y. N. Takayabu, 2007: Westerly wind bursts and their relationship with intraseasonal variations and ENSO. Part I: Statistics. *Mon. Wea. Rev.*, **135,** 3325-3345.

Thompson, C. J., and D. S. Battisti, 2000: A Linear Stochastic Dynamical Model of ENSO. Part I: Development. *J. Climate*, **13,** 2818-2832.

Thompson, C. J. a. D. S. Battisti, 2001: A Linear Stochastic Dynamical Model of ENSO. Part II: Analysis. *J. Climate*, **14,** 445-466.

Trenberth, K. E., G. W. Branstator, D. Karoly, A. Kumar, N-C. Lau, and C. Ropelewski, 1998: Progress during TOGA in understanding and modeling global teleconnections associated with tropical sea surface temperatures. *J. Geophys. Res.*, **103,** 14,291-14324.

Uppala, S.M., et al., 2005: The ERA-40 re-analysis. *Quart. J. R. Meteorol. Soc.*, **131**, 2961-3012. doi:10.1256/qj.04.176.

Vecchi, G. A., and D. E. Harrison, 2000: Tropical Pacific sea surface temperature anomalies, El Niño and equatorial westerly wind events. *J. Climate*, **13,** 1814-1830.

Vimont, D. J., 2002: The seasonal footprinting mechanism in the coupled CSIRO general circulation models and in observations. Ph. D. thesis, Department of Atmospheric Sciences, University of Washington, Seattle, WA.

Vimont, D. J., D. S. Battisti, and A. C. Hirst, 2001: Footprinting: A seasonal link between the mid-latitudes and tropics. *Geophys. Res. Lett.*, **28,** 3923 – 3926.

Vimont, D. J., D. S. Battisti, and A. C. Hirst, 2003a: The seasonal footprinting mechanism in the CSIRO general circulation models. *J Climate*, **16,** 2653–2667.

Vimont, D. J., J. M. Wallace, and D. S. Battisti 2003b: The seasonal footprinting mechanism in the Pacific: Implications for ENSO. *J. Climate*, **16,** 2668 – 2675.

Vimont, D. J., M. Alexander, and A. Fontaine, 2009: Mid-latitude excitation of tropical variability in the Pacific: the role of thermodynamic coupling and seasonality. *J. Climate***, 22**, 518-534.

Walker, G. T. and E. W. Bliss, 1932: World Weather V. *Mem. Roy. Met. Soc.*, **4,** 53-84.

Wu, L., and C. Li, 2007: Warming of the North Pacific Ocean: Local air–sea coupling and remote climatic impacts. *J. Climate*, **20,** 2581–2601.

Wyrtki, K., 1975: El Niño - the dynamic response of the equatorial Pacific Ocean to atmospheric forcing. *J. Phys. Oceanog.*, **5,** 572-584.

Xie, S.-P., 1996: Westward propagation of latitudinal asymmetry in a coupled ocean–atmosphere model. *J. Atmos. Sci.,* **53,** 3236–3250.

Xie, S.-P., 1997: Unstable transition of the tropical climate to an equatorially asymmetric state in a coupled ocean–atmosphere model. *Mon. Wea. Rev.,* **125,** 667–679.

Xie, S.-P., 1999: A dynamic ocean–atmosphere model of the tropical Atlantic decadal variability. *J. Climate*, **12,** 64–70.

Xie, S.-P., and J. A. Carton, 2004: Tropical Atlantic variability: Patterns, mechanisms, and impacts. *In Earth Climate: The Ocean-Atmosphere Interaction*, C. Wang, S.-P. Xie, and J.A. Carton (eds.), Ed., AGU Geophysical Monograph, Washington D.C.

Xie, S.-P., and S. G .H. Philander 1994: A coupled ocean-atmosphere model of relevance to the ITCZ in the eastern Pacific. *Tellus*, **46A,** 340-350.

Xue, Y., M. A. Cane, and S. E. Zebiak, 1997: Predictability of a Coupled Model of ENSO Using Singular Vector Analysis. Part I: Optimal Growth in Seasonal Background and ENSO Cycles. *Mon. Wea. Rev.*, **125,** 2043–2056.

Yu, L., and M. M. Rienecker, 1998: Evidence of an extratropical atmospheric influence during the onset of the 1997–8 El Niño. *Geophys. Res. Lett.*, **25,** 3537–3540.

Zavala-Garay, J., C. Zhang, A. M. Moore, A. T. Wittenberg, M. J. Harrison, A. Rosati, J. Vialard, and R. Kleeman, 2008: Sensitivity of hybrid ENSO models to unresolved atmospheric variability. *J. Climate*, **21,** 3704–3721

Zebiak, S. E., and M. A. Cane, 1987: A model El Nino-Southern Oscillation. *Mon. Wea. Rev.*, **115,** 2262-2278.

Zhang, L., P. Chang, and L. Ji, 2009a: Linking the Pacific Meridional Mode to ENSO: coupled model analysis. *J Climate***,** in press.

Zhang, L., P. Chang, and M. K. Tippett, 2009b: Linking the Pacific Meridional Mode to ENSO: Utilization of a noise filter. *J. Climate*, **22,** 905-922.

Figure Captions

Fig. 1. The SFM simulated in a 100-year integration of the CCM3-RGO-ML model as indicated by: a) the concurrent regression of SLP [contour interval (CI) 0.25 mb per std dev] and Q_{net} [color shading interval (CSI) is 1 Wm^{-2} per std dev, positive into ocean) on the NPO time series - the second PC of SLP for EOFs computed over the North Pacific (20°N-90°N, 110°E-70°W) during November-March; and lagged regressions of SST (shaded), thermocline depth (CI 1m) and wind (vectors) in the tropical Pacific on the NPO time series for the following b) JFM, c) AMJ, d) JAS and e) ONDJF. The SST and wind scales are located at the bottom of the figure and the upper fight corner of panels b)-e), respectively.

Fig. 2. The NPO-related heat flux forcing added in each of the 60 branch experiments derived from the 2nd EOF of SLP over the North Pacific in an extended AGCM simulation with repeating climatological SSTs. The forcing is obtained by doubling the Q_{net} values (CSI is 5 Wm^{-2}) from 20°S-65°N, 110°E-70°W in the Pacific regressed onto the 2nd PC of SLP during NDJFM, which corresponds to a 2σ NPO anomaly in its negative phase (see Fig. 1a).

Fig. 3. Evolution of the response to the "negative" phase of the NPO-related forcing. The ensemble mean difference (Δ) between the "Qflux" experiment (Exp) and control (Cntrl) simulations for (left) SST (CI is 0.1°C) and (right) 1000 mb wind (vectors, m s^{-1}) and latent heat flux (Q_{lh} Wm^{-2}). The response is shown, from top to bottom, for JFM(0), AMJ(0), JAS(0) and OND(1), where 0 denotes the initial year of the integration and 1 the

following year. Stippling denotes grid squares where t-tests indicate that the SST and Q_{lh} from the 60 Exp simulations are significantly different from the control at the 95% level.

Fig. 4. As in Fig. 3, but for the thermocline depth (Δh, CI 1m for $|h| < 6$ and 2 m for $|h| > 6$)) and Ekman pumping ($W_{ek}=\nabla\times\boldsymbol{\tau}/\rho f$, positive upward, CSI is 1.0 x10^{-6} ms^{-1}), which is not plotted within 2° of the equator where it goes to infinity. Stippling denotes areas where Δh is statistically significant.

Fig. 5 The response in precipitation (ΔP, CI & CSI are 4 cm per 90 days) during AMJ(0). Stippling denotes areas that are statistically significant.

Fig. 6. The SST response (CI & CSI are 0.1°C) during OND(1) to the heat flux forcing associated with the alternate ("positive") phase of the NPO.

Fig. 7. Hövmoller diagrams of a) ΔQ_{lh} (CSI is 2 Wm^{-2}) and b) ΔU (CSI is 0.1 ms^{-1}); ΔSST (CI is 0.1°C) is shown in both (a) and (b). (c) The Hövmoller path consists of three sections: *i)* 25°N, 155°W extending southwest to 12°N, 165°W; *ii)* south along 165°W to the equator and *iii)* east along the equator to 85°W; corresponding to points *i)* 0-5, *ii)* 5-10 and *iii)* 10-26, respectively along the entire transect. All values are derived from Exp-Cntrl 5-day running means averaged over three grid values including the points on and to either side of the transect line.

Fig. 8. Similar to Fig. 6 but for Hövmoller diagram of (a) Δh (CI/CSI is 1 m) consisting of three sections shown in (b) that form a counterclockwise circuit around the tropical Pacific which extend: from *i)* east to west averaged over 3°N-7°N; *ii)* 5°N south to the equator averaged over 130°-135°E and *iii)* west to east averaged over to 2°N-2°S.

Fig. 9. Bar chart of the Exp – Cntrl (Δ) SST (°C) during NDJ(1) in the Nino 3.4 region for each of the 60 branch simulations numbered by the order the year they occur in the control run.

Fig. 10. Scatter plot of ΔSST verses the corresponding SST anomaly (′) relative to the long-term mean in the Cntrl during NDJ(1) in the Nino 3.4 region. The 60 cases are numbered by the year they occur in the control. The eight simulations with the largest or "warm" response are shown in red while eight years with similar SST′ values but near zero ΔSST, termed "neutral" cases, are shown in blue.

Fig. 11. SST (shading) and *h* (contours) changes in the neutral (a)-(c) composite. The departures from the mean (′) in the Cntrl in a) NDJ(0) and b) NDJ(1) with no additional forcing and the difference (Δ) from the Cntrl in c) NDJ(1) when NPO forcing is added. Arrows denote change from the winter of yr(0) to yr(1). b)-f) show the SST changes but for the warm composite. The SST CSI is 0.2°C and *h* CI is 4 m and in all panels.

Fig. 12. The ΔSST (CI & CSI is 0.2°C) for the a) neutral and b) warm composite, and the Δh (CI & CSI is 2 m) for the c) neutral and warm composite d) in Mar(0).

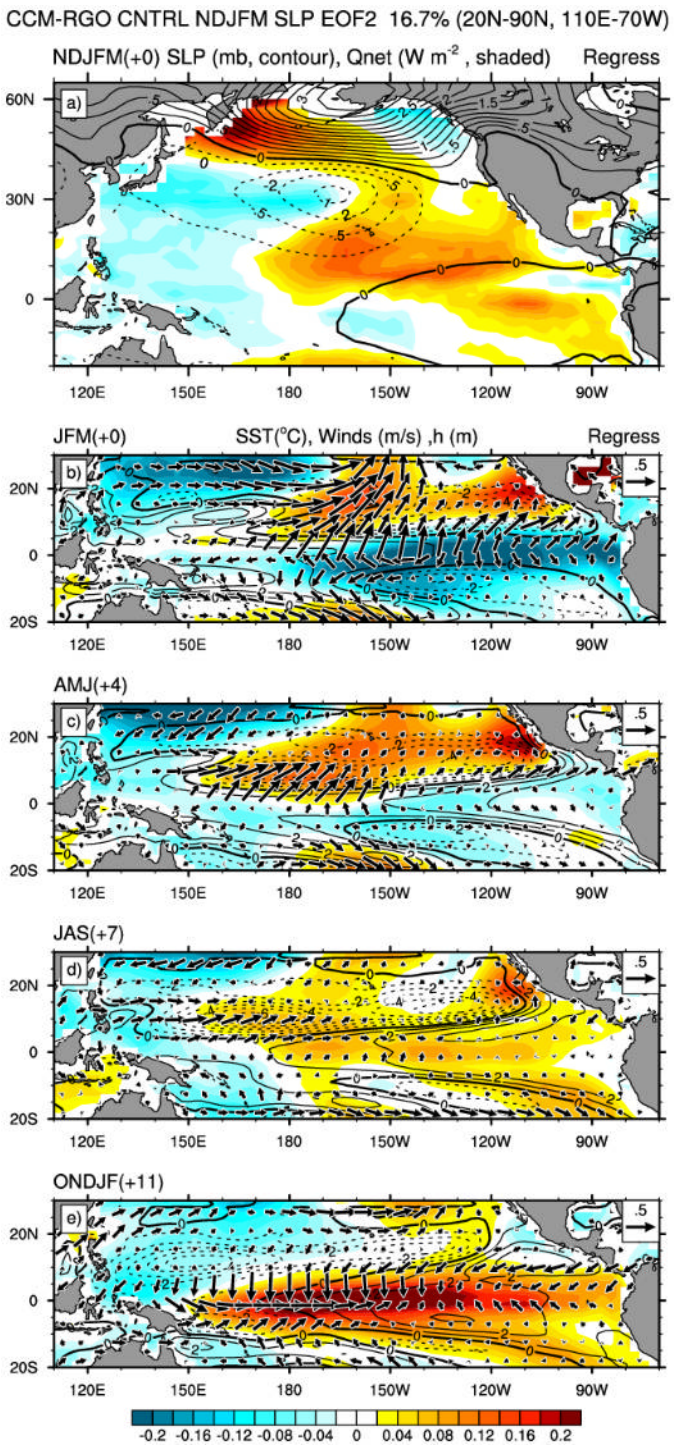

Fig. 1. The SFM simulated in a 100-year integration of the CCM3-RGO-ML model as indicated by: a) the concurrent regression of SLP [contour interval (CI) 0.25 mb per std dev] and Q_{net} [color shading interval (CSI) is 1 Wm^{-2} per std dev, positive into ocean) on the NPO time series - the second PC of SLP for EOFs computed over the North Pacific (20°N-90°N, 110°E-70°W) during November-March; and lagged regressions of SST (shaded), thermocline depth (CI 1m) and wind (vectors) in the tropical Pacific on the NPO time series for the following b) JFM, c) AMJ, d) JAS and e) ONDJF. The SST and wind scales are located at the bottom of the figure and the upper fight corner of panels b)-e), respectively.

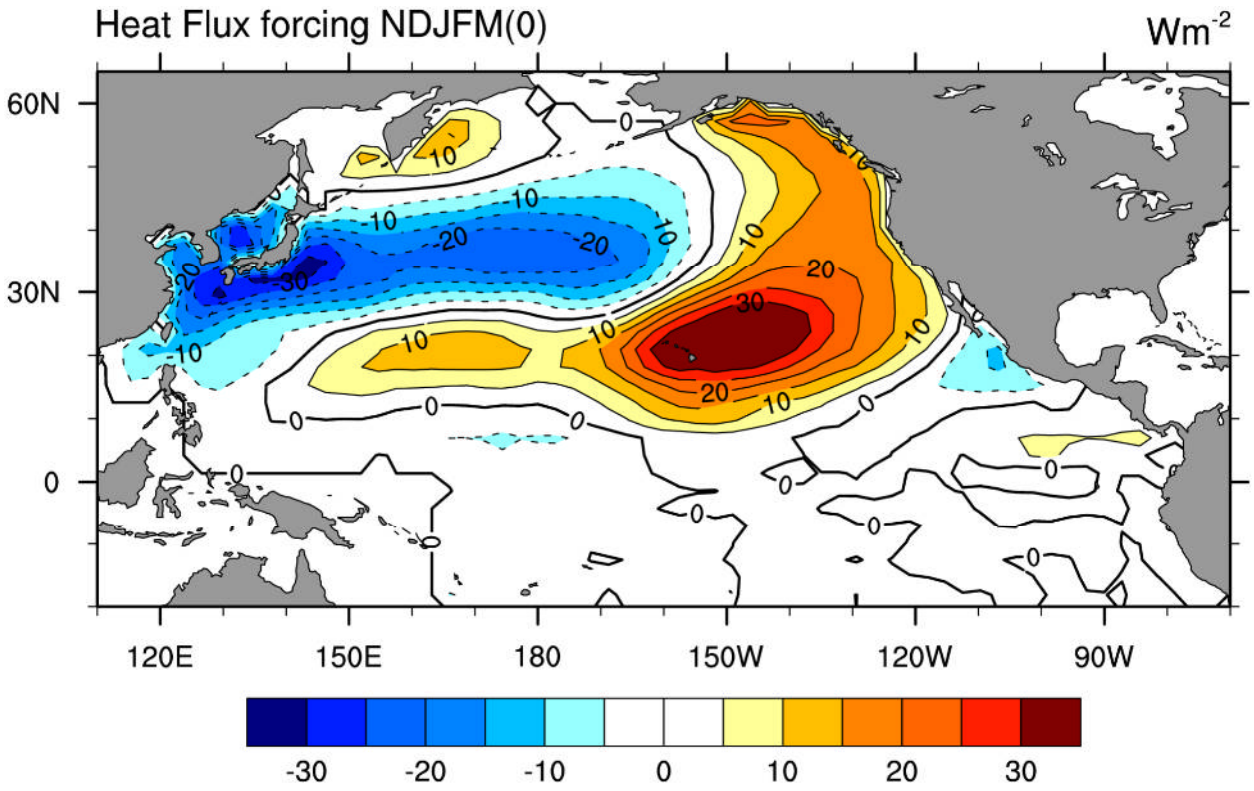

Fig. 2. The NPO-related heat flux forcing added in each of the 60 branch experiments derived from the 2nd EOF of SLP over the North Pacific in an extended AGCM simulation with repeating climatological SSTs. The forcing is obtained by doubling the Q_{net} values (CI & CSI are 5 Wm^{-2}) from 20°S-65°N, 110°E-70°W in the Pacific regressed onto the 2nd PC of SLP during NDJFM, which corresponds to a 2 standard deviation NPO anomaly in its negative phase (see Fig. 1a).

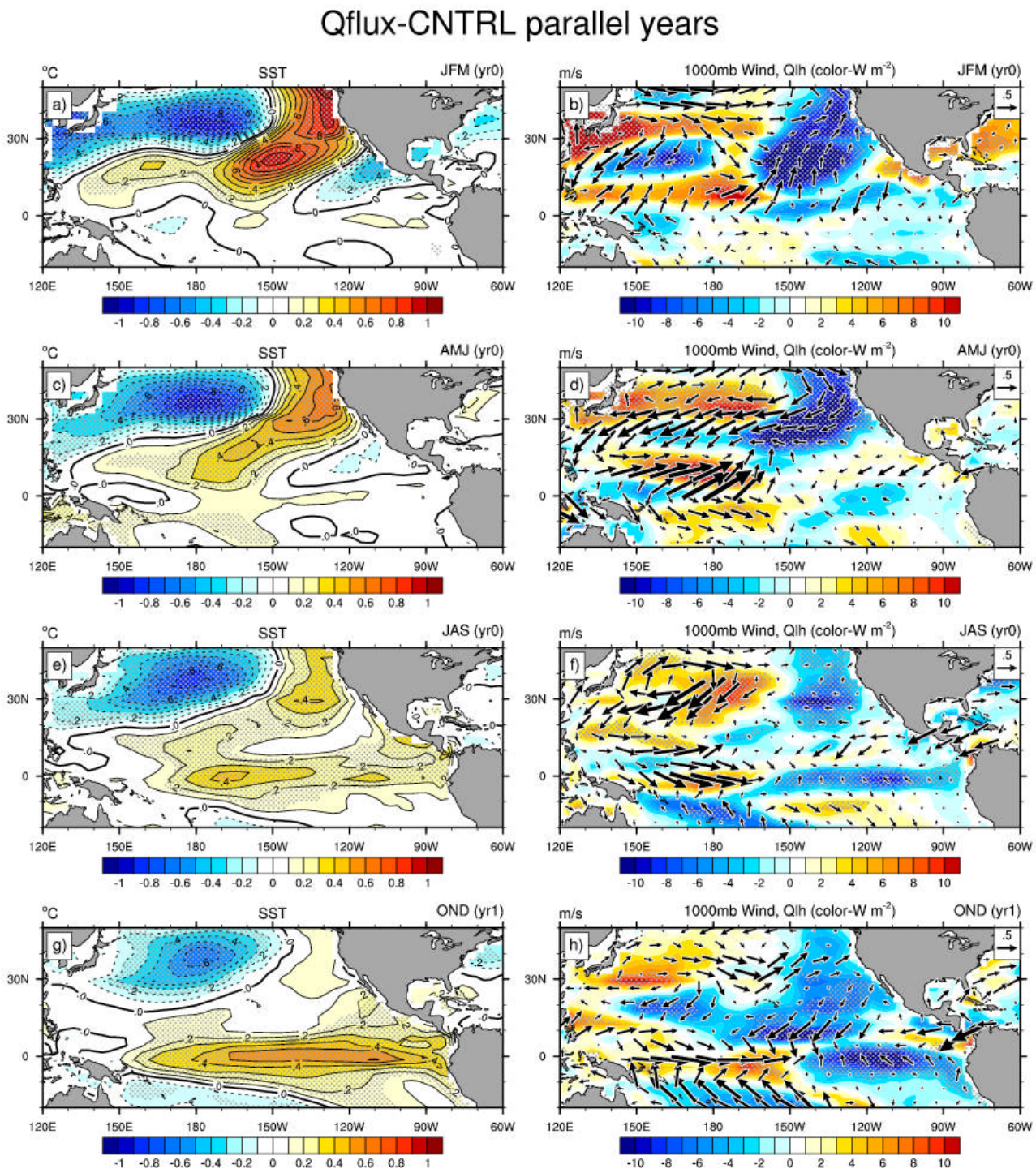

Fig. 3. Evolution of the response to the "negative" phase of the NPO-related forcing. The ensemble mean difference (Δ) between the "Qflux" experiment (Exp) and control (Cntrl) simulations for (left) SST (CI is 0.1°C) and (right) 1000 mb wind (vectors, m s^{-1}) and latent heat flux (Q_{lh} Wm^{-2}). The response is shown, from top to bottom, for JFM(0), AMJ(0), JAS(0) and OND(1), where 0 denotes the initial year of the integration and 1 the following year. Stippling denotes grid squares where t-tests indicate that the SST and Q_{lh} from the 60 Exp simulations are significantly different from the control at the 95% level.

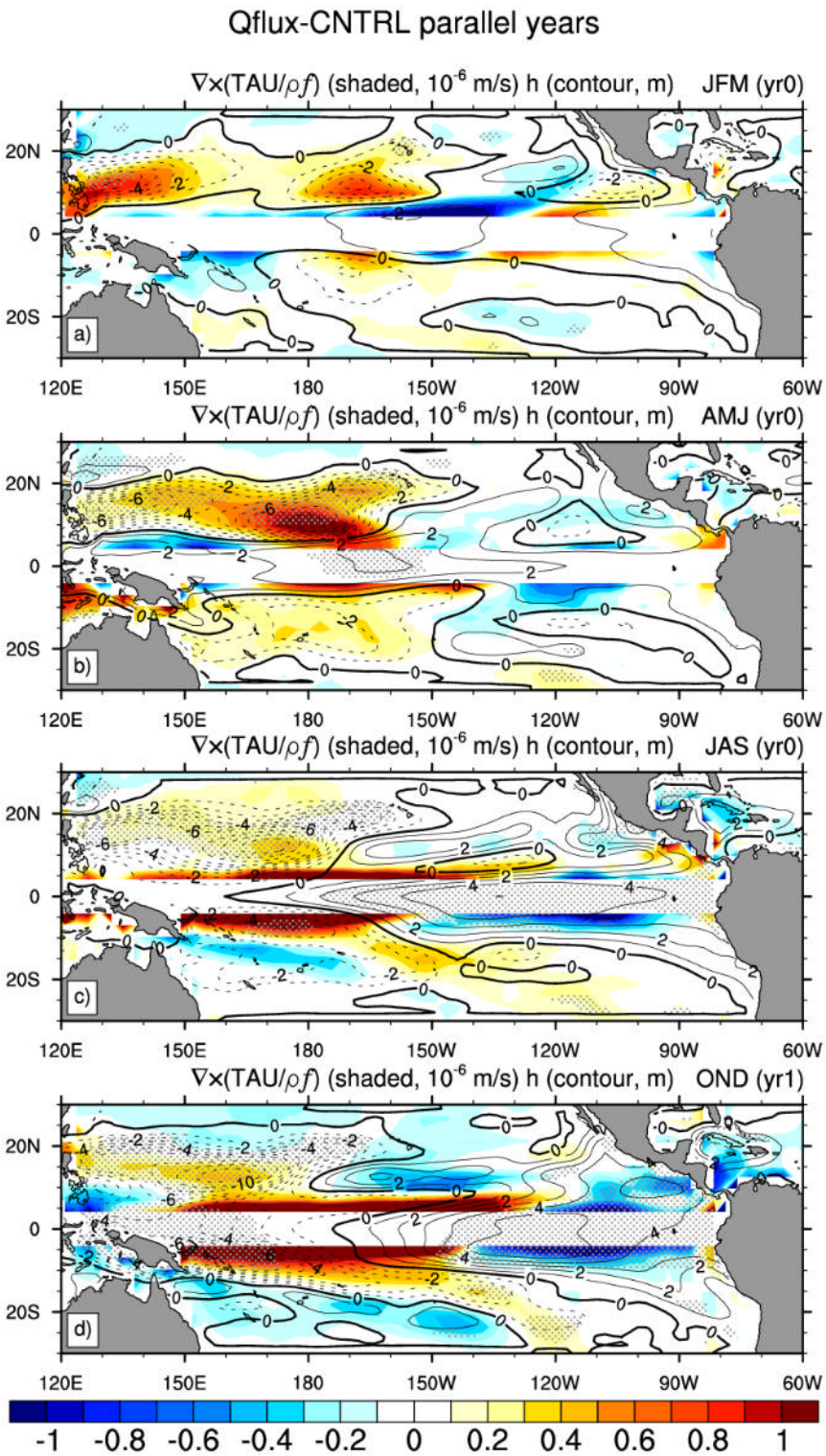

Fig. 4. As in Fig. 3, but for the thermocline depth (Δh, CI 1m for $|h| < 6$ and 2 m for $|h| > 6$)) and Ekman pumping ($W_{ek}=\nabla\times\boldsymbol{\tau}/\rho f$, positive upward, CSI is 1.0 x10^{-6} ms^{-1}), which is not plotted within 2° of the equator where it goes to infinity. Stippling denotes areas where Δh is statistically significant.

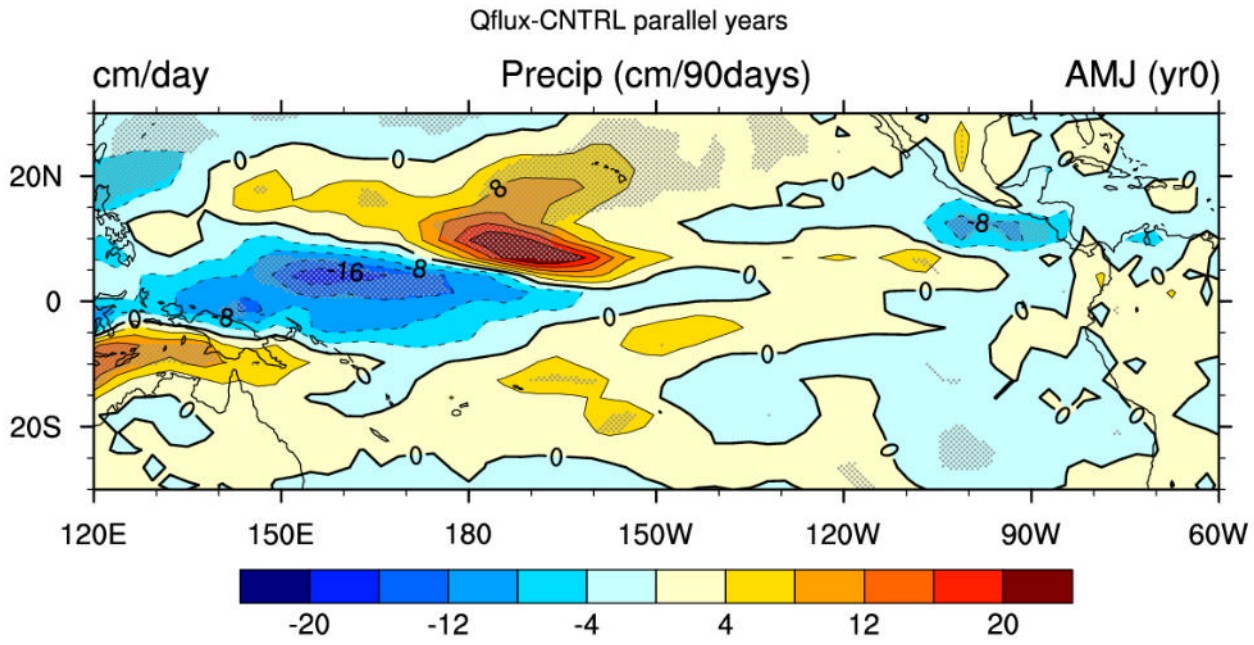

Fig. 5 The response in precipitation (ΔP, CI&CSI are 4 cm per 90 days) during AMJ(0). Stippling denotes areas that are statistically significant.

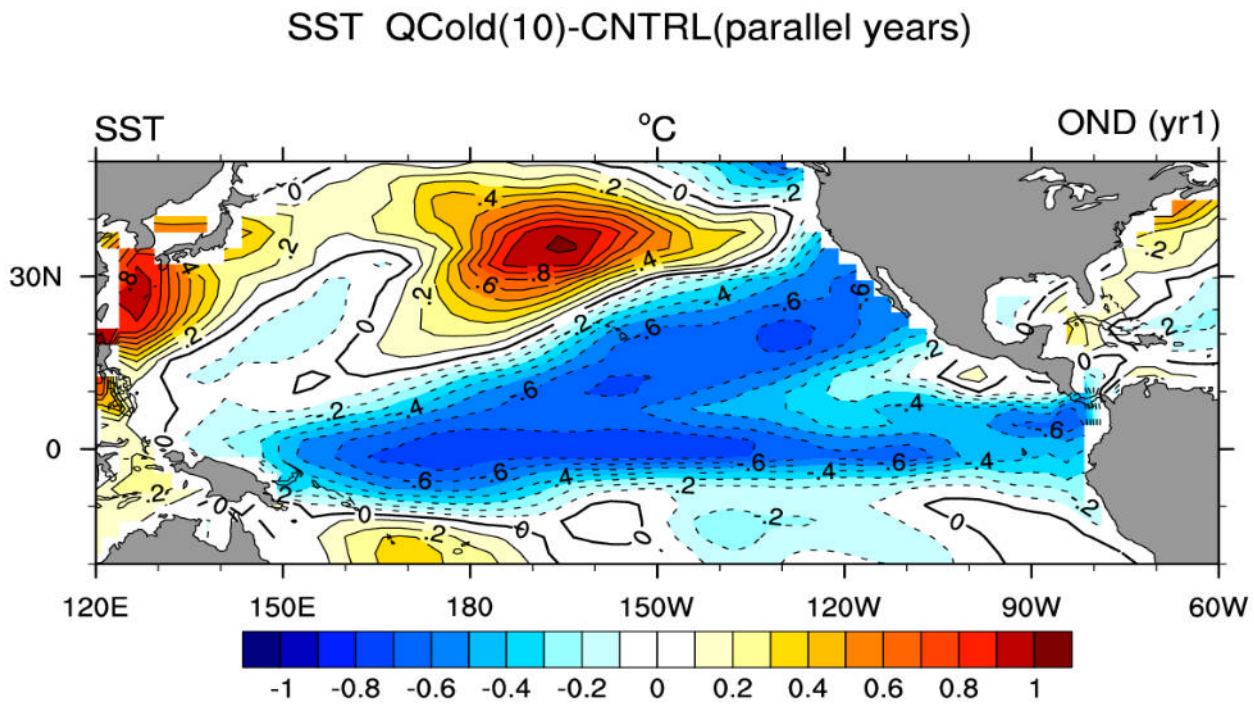

Fig. 6 The SST response (CI&CSI are 0.1°C) during OND(1) to the heat flux forcing associated with the alternate ("positive") phase of the NPO.

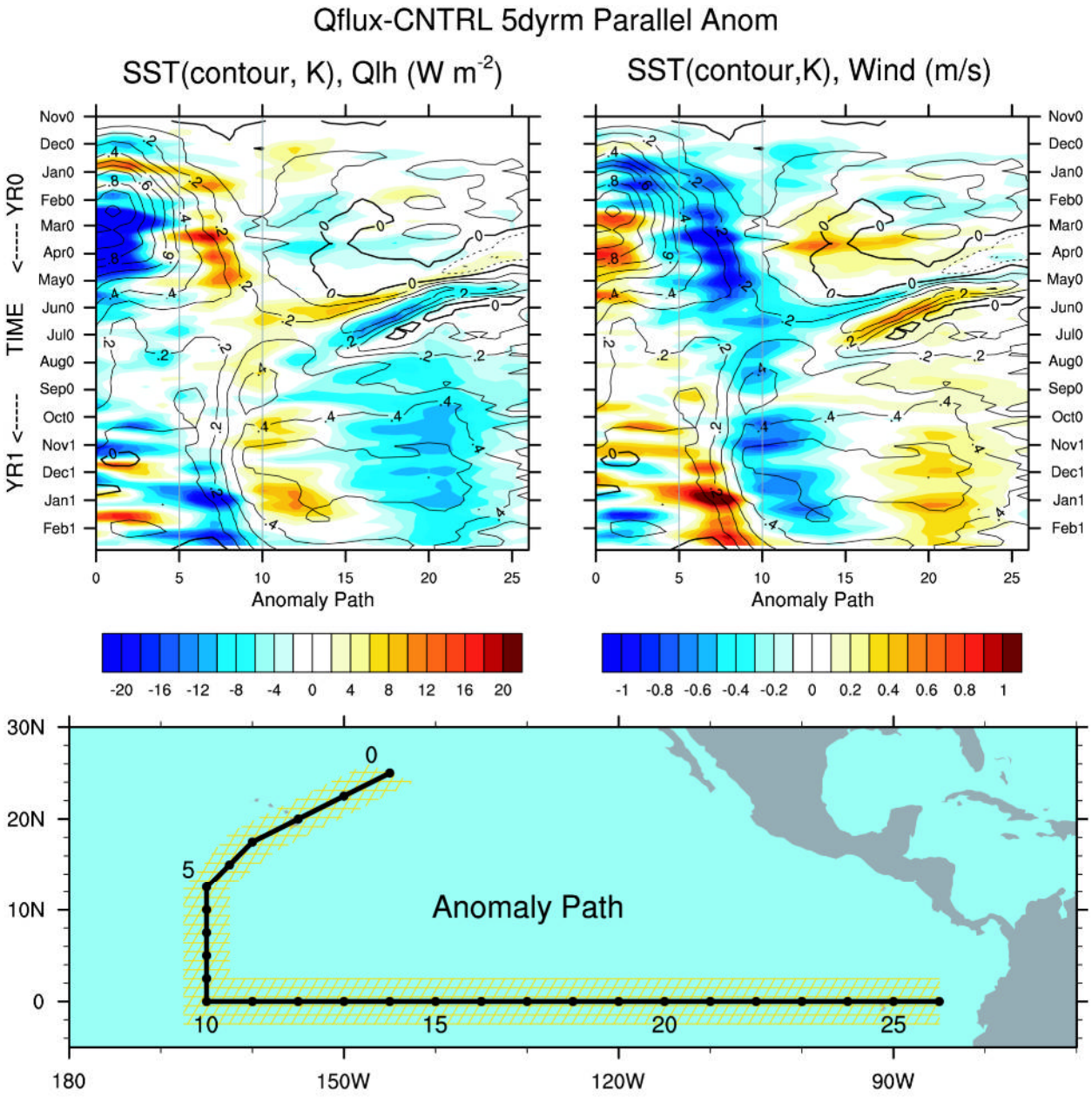

Fig. 7. Hövmoller diagrams of a) ΔQ_{lh} (CSI is 2 Wm^{-2}) and b) ΔU (CSI is 0.1 ms^{-1}); ΔSST (CI is 0.1°C) is shown in both (a) and (b). (c) The Hövmoller path consists of three sections: *i)* 25°N, 155°W extending southwest to 12°N, 165°W; *ii)* south along 165°W to the equator and *iii)* east along the equator to 85°W; corresponding to points *i)* 0-5, *ii)* 5-10 and *iii)* 10-26, respectively along the entire transect. All values are derived from Exp-Cntrl 5-day running means averaged over three grid values including the points on and to either side of the transect line.

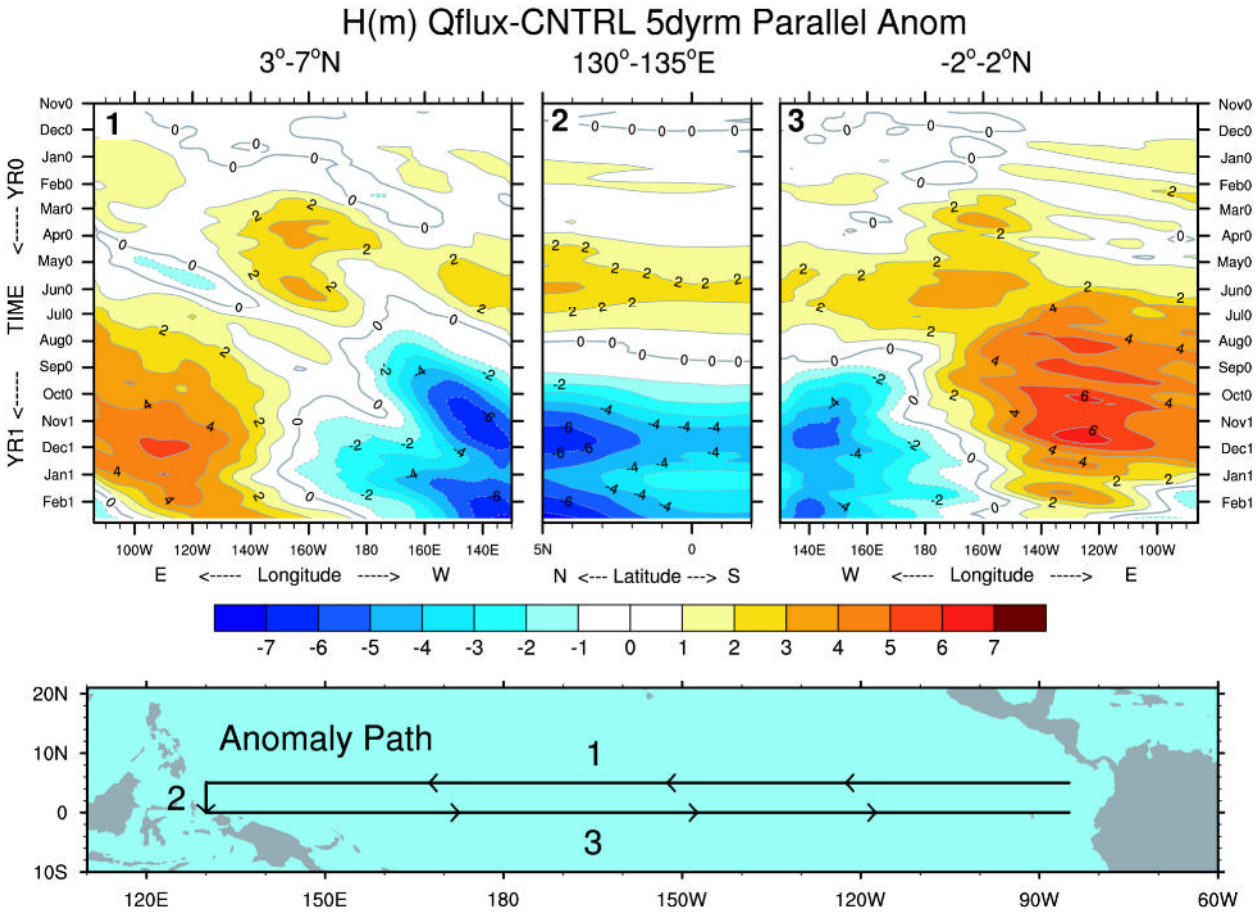

Fig. 8. Similar to Fig. 6 but for Hövmoller diagram of (a) Δh (CI & CSI are 1 m) consisting of three sections shown in (b) that form a counterclockwise circuit around the tropical Pacific which extend: from *i)* east to west averaged over 3°N-7°N; *ii)* 5°N south to the equator averaged over 130°-135°E and *iii)* west to east averaged over to 2°N-2°S.

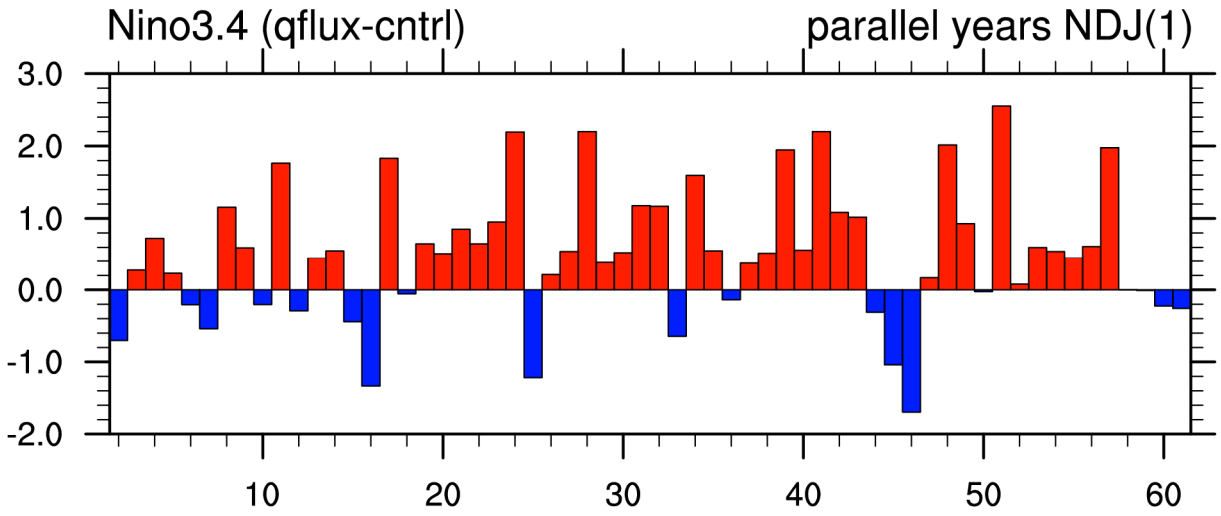

Fig. 9. Bar chart of the Exp – Cntrl (Δ) SST (°C) during NDJ(1) in the Nino 3.4 region for each of the 60 branch simulations numbered by the order the year they occur in the control run.

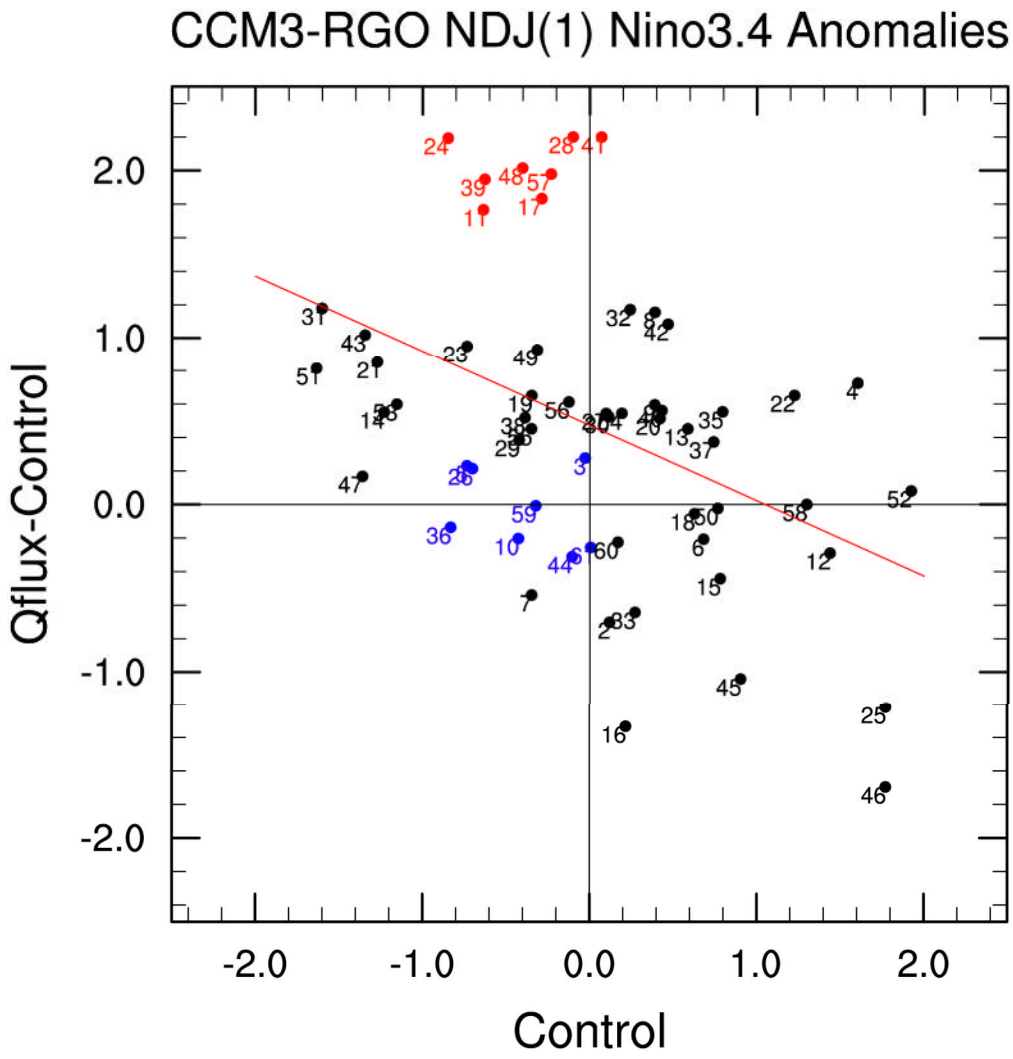

Fig. 10. Scatter plot of ΔSST verses the corresponding SST anomaly (′) relative to the long-term mean in the Cntrl during NDJ(1) in the Nino 3.4 region. The 60 cases are numbered by the year they occur in the control. The eight simulations with the largest or "warm" response are shown in red while eight years with similar SST′ values but near zero ΔSST, termed "neutral" cases, are shown in blue.

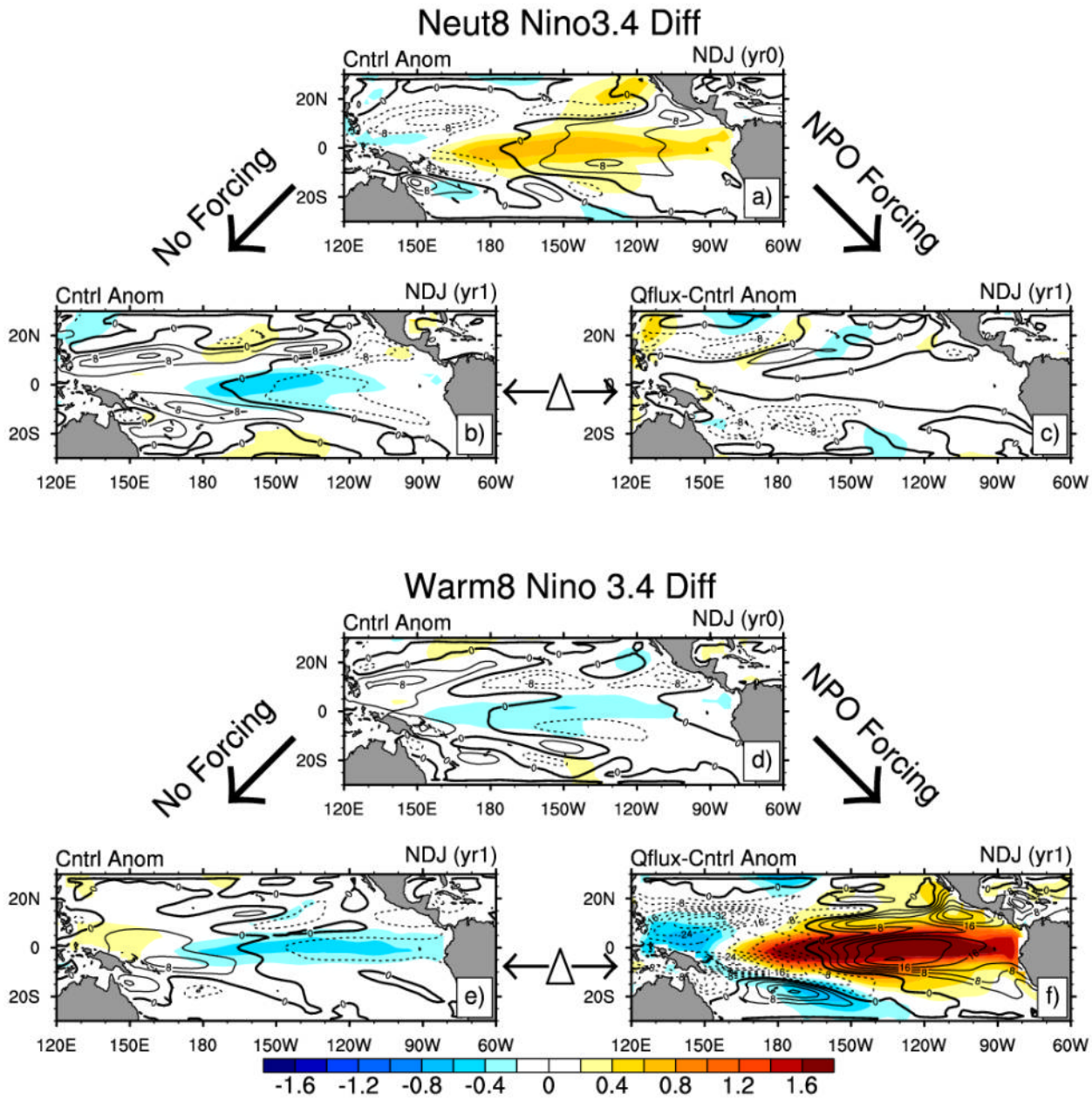

Fig. 11. SST (shading) and *h* (contours) changes in the neutral (a)-(c) composite. The departures from the mean (′) in the Cntrl in a) NDJ(0) and b) NDJ(1) with no additional forcing and the difference (Δ) from the Cntrl in c) NDJ(1) when NPO forcing is added. Arrows denote change from the winter of yr(0) to yr(1). b)-f) show the SST changes but for the warm composite. The SST CSI is 0.2°C and *h* CI is 4 m and in all panels.

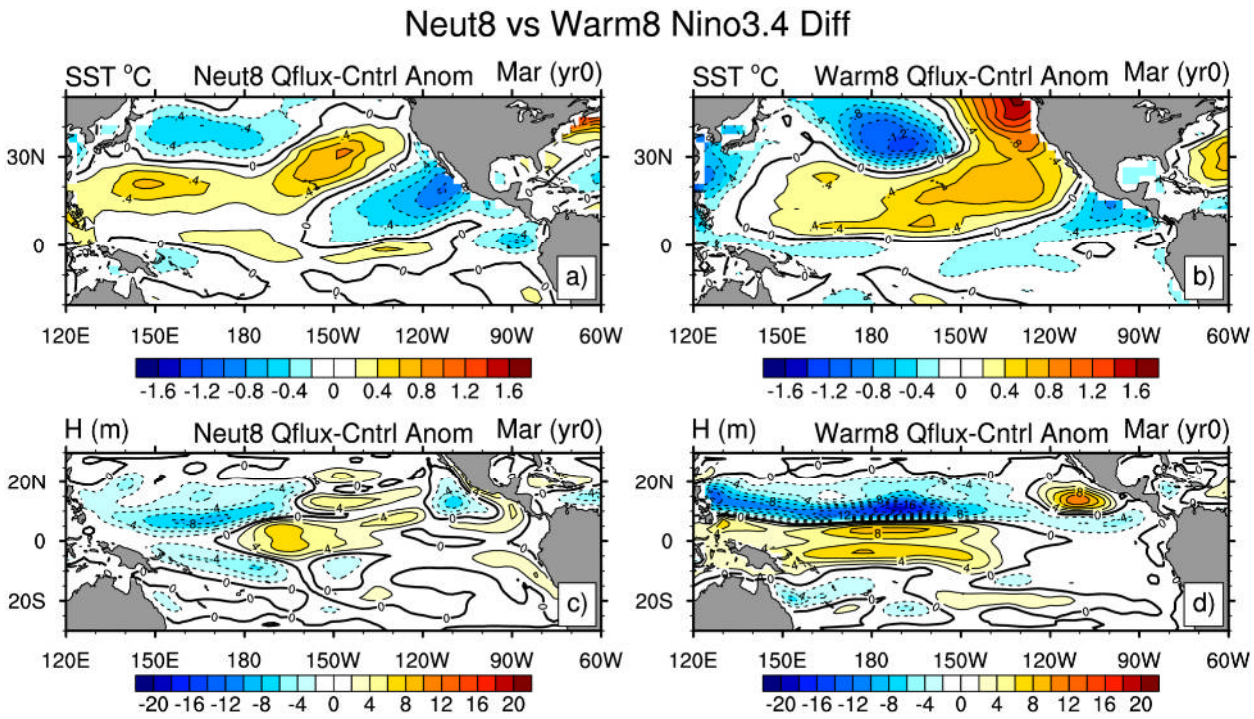

Fig. 12. The ΔSST (CI & CSI is 0.2°C) for the a) neutral and b) warm composite, and the Δ*h* (CI & CSI is 2 m) for the c) neutral and warm composite d) in Mar(0).